Decay of Higher Order Solitons in the presence of Dispersion, Self-steeping & Raman Scattering

Thesis submitted in partial fulfillment of the requirement for the award of the degree of

MASTER OF ENGINEERING

In

ELECTRONICS & COMMUNICATION ENGINEERING

Submitted by

Vidhu Rawal

Roll no. 800961021

Under the Guidance of

Dr. Sanjay Sharma

Associate Professor

Electronics and Communication Engineering Department

Thapar University, Patiala-147004 (PUNJAB)

July-August 2011

CERTIFICATE

I hereby declare that the work which is being presented in the thesis entitled **"Decay of higher order Solitons in the presence of Dispersion, Self-Steeping & Raman scattering"** in the partial fulfilment for the award of **Masters of Engineering** in **Electronics & Communication Engineering** from **Thapar University** is an authentic record of my own work carried under the supervision and guidance of **Dr. Sanjay Sharma,** Associate Professor, Department of Electronics & Communication Engineering.

Dated:

(Vidhu Rawal)

This is to certify that the above statement made by the candidate is correct and true to the best of my knowledge and belief.

6/8/2011

Dr. SANJAY SHARMA,

Associate Professor,

Thesis Supervisor,

Thapar University,

Patiala-147004

Counter Signed by:

17/8

Dr. A.K.CHATTERJEE

Professor & Head,

E.C.E.D., Thapar University,

Patiala-147004

Dr. S.K.MOHAPATRA

Dean of Academic Affairs,

Thapar University,

Patiala-147004

ACKNOWLEDGEMENT

No volume of words is enough to express my gratitude towards my guide, **Dr. Sanjay Sharma**, Associate Professor, Electronics and Communication Engineering Department, Thapar University, who has been very concerned and has aided for all the material essential for the preparation of this thesis report. He has helped me to explore this vast topic in an organized manner and provided me with all the ideas on how to work towards a research-oriented venture.

I am also thankful to **Dr. A. K. Chatterjee**, Head of Department, ECED and **Ms. Alpana Aggarwal**, P.G. Coordinator, for the motivation and inspiration that triggered me for the thesis work.

I would also like to thank the staff members and my colleagues who were always there in the need of the hour and provided with all the help and facilities, which I required, for the completion of my thesis.

Most importantly, I would like to thank my parents and the Almighty for showing me the right direction out of the blue, to help me stay calm in the oddest of the times and keep moving even at times when there was no hope.

Vidhu Rawal

Roll No. – 800961021

ABSTRACT

The decay of higher order solitons in optical fiber by the influence of the Dispersion, Raman Scattering & Self steeping nonlinear susceptibilities is theoretically analyzed. This influence on the dynamics of optical solitons decay is explored theoretically and experimentally. We have taken into account higher-order dispersion, the shock (self-steepening) term, and a term describing the Raman self-pumping of an ultra short pulse. We study the decay of higher order solitons in optical fibers. The effect of self-steepening, dispersion & Raman scattering on higher-order solitons is remarkable in that it leads to breakup of such solitons into their constituents, a phenomenon referred to as soliton decay. In this phenomenon, the two solitons gets separated from each other within a distance of two soliton periods and continue to move apart with further propagation inside the fiber.

It is shown that the Raman Effect is dominant on a femtosecond time scale and leads to the decay of higher-order solitons. For the case of the $N = 2$ soliton an intense pulse at a distinctly Stokes-shifted frequency is created. This pulse eventually shapes into a fundamental soliton, and its further evolution is governed by the combination of dispersion, self-phase modulation, and the soliton self-frequency shift. The theoretical results are in good quantitative agreement with the recent experiments.

TABLE OF CONTENTS

LIST OF FIGURES

soliton number, N, and so only partial spectral re-compression occurs

FIGURE 3.3 Temporal separation of the N=3 soliton spectral components as a result of a perturbation applied at the half soliton period distance. The perturbation reduces the value of the soliton number, N, and so only partial spectral re-compression occurs

FIGURE 3.4 Maximum obtainable wavelength separations $\Delta\lambda max$ as functions of input pulse width for N=2 (solid curve) and N=3 (dashed curve) solitons. The corresponding frequency separations at 1.55 μm wavelength are indicated on the right vertical axis

FIGURE 3.5 Numerical results, showing the decay of an N=2 soliton, initiated by a step increasing the dispersion from 8 ps/nm-km to 16 ps/nm-km at the position, z/z0=0.5. Temporal (a) and spectral (b) evolution on next page show the formation of nearly fundamental solitons at two wavelengths

FIGURE 3.6 Numerical results, showing the decay of an N=3 soliton, initiated by a step increasing the dispersion from 8 ps/nm-km to 16 ps/nm-km at the position, z/z0=0.25. Temporal (a) and spectral (b) evolution on next page show the formation of nearly fundamental solitons at three wavelengths

FIGURE 3.7 Numerical results, showing the decay of an N=2 soliton, initiated by attenuation (3dB) at the position, z/z0=0.5. Temporal (a) and spectral (b) evolution on next page show the formation of sub pulses at two wavelengths

FIGURE 3.8 Numerical results, showing the decay of an N=2 soliton, initiated by band pass filtering ($\Delta\lambda f / \Delta\lambda in = 2.72$) at the position, z/z0=0.5. Temporal (a) and spectral (b) evolution on next page show the formation of sub pulses at two wavelengths

FIGURE 3.9 Wavelength separations obtained as functions of dispersion difference (a), attenuation (b), and filter bandwidth (c) for N=2 solitons (solid curves) and N=3 solitons (dashed curves). Wavelength separation and filter bandwidth are normalized with respect to the input FWHM spectral width

LIST OF ABBREVIATIONS

SSFM -- Split-Step Fourier Method

NLSE -- Non-Linear Schödinger Equation

MNLSE -- Modified Non-Linear Schödinger Equation

ASE -- Amplified Spontaneous Emission

GVD -- Group-Velocity Dispersion

SPM -- Self-Phase Modulation

OSA -- Optical Spectrum Analyzer

EDFA -- Erbium-Doped Fiber Amplifier

LDF -- Low Dispersion Fiber

HDF -- High Dispersion Fiber

NDF -- Negative Dispersion Fiber

DCF -- Dispersion Compensating Fiber

MFD -- Mode Field Diameter

CHAPTER 1

INTRODUCTION

This introductory chapter is intended to provide an overview of the fiber characteristics that are important for understanding the nonlinear effects discussed later on. Among the nonlinear effects that have been studied extensively using optical fibers as a nonlinear medium are self-phase modulation, cross-phase modulation, four-wave mixing, stimulated Raman scattering, and stimulated Brillouin scattering.

1.1 Historical Perspective

Total internal reflection—the basic phenomenon responsible for guiding of light in optical fibers—is known from the nineteenth century [1]. Although uncladded glass fibers were fabricated in the 1920s [2]-[4], the field of fiber optics was not born until the 1950s when the use of a cladding layer led to considerable improvement in the fiber characteristics [5]- [8]. The idea that optical fibers would benefit from a dielectric cladding was not obvious and has a remarkable history [1].

The field of fiber optics developed rapidly during the 1960s, mainly for the purpose of image transmission through a bundle of glass fibers [9]. These early fibers were extremely lossy (loss > 1000 dB/km) from the modern standard. However, the situation changed drastically in 1970 when, following an earlier suggestion [10], losses of silica fibers were reduced to below 20 dB/km [11]. Further progress in fabrication technology resulted by 1979 in a loss of only 0.2 dB/km in the 1.55-μm wavelength region [13], a loss level limited mainly by the fundamental process of Rayleigh scattering.

The availability of low-loss silica fibers led not only to a revolution in the field of optical fiber communications [14]-[17] but also to the advent of the new field of nonlinear fiber optics. Stimulated Raman- and Brillouin-scattering processes in optical fibers were studied as early as 1972 [18]- [20]. This work stimulated the study of other nonlinear phenomena such as optically induced birefringence, parametric four-wave mixing, and self-phase modulation [20]-[25]. An important contribution was made in 1973 when it was suggested that optical fibers can support soliton-like pulses as a result of interplay between the dispersive and

nonlinear effects [26]. Optical solitons were observed in a 1980 experiment [27] and led to a number of advances during the 1980s in the generation and control of ultra short optical pulses [28]-[32]. The decade of the 1980s also saw the development of pulse-compression and optical-switching techniques that exploited the nonlinear effects in fibers. Pulses as short as 6 fs were generated by 1987. Several reviews and books cover the enormous progress made during the 1980s .

The field of nonlinear fiber optics continued to grow during the decade of the 1990s. A new dimension was added when optical fibers were doped with rare-earth elements and used to make amplifiers and lasers. Although fiber amplifiers were made as early as 1964, it was only after 1987 that their development accelerated. Erbium-doped fiber amplifiers attracted the most attention because they operate in the wavelength region near 1.55 μm and can be used for compensation of losses in fiber-optic light wave systems. Such amplifiers were used for commercial applications beginning in 1995. Their use has led to a virtual revolution in the design of multichannel light wave systems [14]-[17].

The advent of fiber amplifiers also fueled research on optical solitons and led eventually to the concept of dispersion-managed solitons. In another development, fiber gratings, first made in 1978, were developed during the 1990s to the point that they became an integral part of light wave technology. Nonlinear effects in fiber gratings and photonic-crystal fibers have attracted considerable attention since 1996. Clearly, the field of nonlinear fiber optics has grown considerably in the 1990s and is expected to do so during the twenty-first century. It has led to a number of advances important from the fundamental as well as the technological point of view. The interest in nonlinear fiber optics should continue in view of the development of the photonic-based technologies for information management.

Fiber Characteristics

In its simplest form, an optical fiber consists of a central glass core surrounded by a cladding layer whose refractive index n_2 is slightly lower than the core indexn_1. Such fibers are generally referred to as step-index fibers to distinguish them from graded-index fibers in which the refractive index of the core decreases gradually from center to core boundary [12]-[14]. Figure 1.1 shows schematically the cross section and refractive-index profile of a step index fiber. Two parameters that characterize an optical fiber are the relative core-cladding index difference

$$\Delta = \frac{n_1 - n_2}{n_1} \quad (1.1)$$

And the so-called *V* parameter defined as

$$V = k_0 a (n_1^2 - n_2^2)^{1/2} \quad (1.2)$$

Where $k_0 = 2\pi/\lambda$, a is the core radius and λ is the wave length of light.

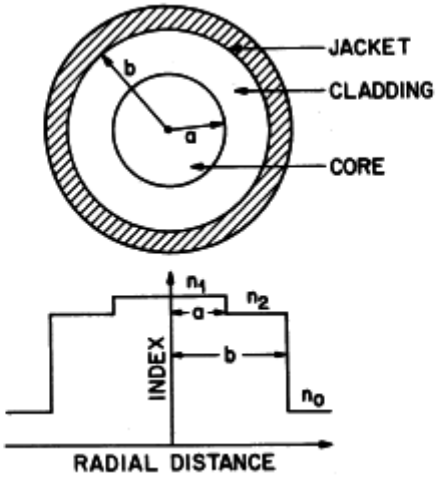

Figure 1.1 Schematic illustration of the cross section and the refractive-index profile of a step-index fiber.

The *V* parameter determines the number of modes supported by the fiber. It is well known that a step-index fiber supports a single mode if *V* < 2:405. Optical fibers designed to satisfy this condition are called single-mode fibers. The main difference between the single-mode and multimode fibers is the core size. The core radius *a* is typically 25–30 μm for multimode fibers.

1.2 Higher-Order Soliton Decay

Fiber Nonlinearities

The response of any dielectric to light becomes nonlinear for intense electromagnetic fields, and optical fibers are no exception. On a fundamental level, the origin of nonlinear response is related to inharmonic motion of bound electrons under the influence of an applied field. As

a result, the total polarization **P** induced by electric dipoles is not linear in the electric field **E**, but satisfies the more general relation [15]-[18].

$$\boldsymbol{P} = \varepsilon_0(x^{(1)}.\boldsymbol{E} + x^{(2)}:\boldsymbol{EE} + x^{(3)}:\boldsymbol{EEE} + \cdots) \quad (1.3)$$

where ε_0 is the vacuum permittivity and $x^{(j)}$ (j =1,;2,…; : : :) is jth order susceptibility. In general, $x^{(j)}$ is a tensor of rank j++1. The linear susceptibility $x^{(1)}$ represents the dominant contribution to **P**. Its effects are included through the refractive index n and the attenuation coefficient α. The second-order susceptibility $x^{(2)}$ is responsible for such nonlinear effects as second-harmonic generation and sum-frequency generation [16]. However, it is nonzero only for media that lack inversion symmetry at the molecular level. As SiO2 is a symmetric molecule, $x^{(2)}$ vanishes for silica glasses. As a result, optical fibers do not normally exhibit second-order nonlinear effects. Nonetheless, the electric-quadrupole and magnetic-dipole moments can generate weak second-order nonlinear effects. Defects or color centers inside the fiber core can also contribute to second-harmonic generation.

Nonlinear Refraction

The lowest-order nonlinear effects in optical fibers originate from the third-order susceptibility$x^{(3)}$, which is responsible for phenomena such as third-harmonic generation, four-wave mixing, and nonlinear refraction. Unless special efforts are made to achieve phase matching, the nonlinear processes that involve generation of new frequencies (e.g. third-harmonic generation and four-wave mixing) are not efficient in optical fibers. Most of the nonlinear effects in optical fibers therefore originate from nonlinear refraction [16], a phenomenon referring to the intensity dependence of the refractive index.

In its simplest form, the refractive index can be written as

$$\tilde{n}(\omega, |E|^2) = n(\omega) + n_2|E|^2 \quad (1.4)$$

Where, $n(\omega)$is the linear part, $|E|^2$ is the optical intensity inside the fiber, and n_2 is the nonlinear-index coefficient related to $x^{(3)}$.

Stimulated Inelastic Scattering

The nonlinear effects governed by the third-order susceptibility $x^{(3)}$ are elastic in the sense that no energy is exchanged between the electromagnetic field and the dielectric medium. A

second class of nonlinear effects results from stimulated inelastic scattering in which the optical field transfers part of its energy to the nonlinear medium. Two important nonlinear effects in optical fibers fall in this category; both of them are related to vibrational excitation modes of silica. These phenomena, known as stimulated Raman scattering (SRS) and stimulated Brillouin scattering (SBS), were among the first nonlinear effects studied in optical fibers [18]-[20]. The main difference between the two is that optical phonons participate in SRS while acoustic phonons participate in SBS.

In a simple quantum-mechanical picture applicable to both SRS and SBS, a photon of the incident field (called the pump) is annihilated to create a photon at a lower frequency (belonging to the Stokes wave) and a phonon with the right energy and momentum to conserve the energy and the momentum. Of course, a higher-energy photon at the so-called anti-Stokes frequency can also be created if a phonon of right energy and momentum is available.

Even though SRS and SBS are very similar in their origin, different dispersion relations for acoustic and optical phonons lead to some basic differences between the two. A fundamental difference is that SBS in optical fibers occurs only in the backward direction whereas SRS can occur in both directions.

Although a complete description of SRS and SBS in optical fibers is quite involved, the initial growth of the Stokes wave can be described by a simple relation. For SRS, this relation is given by

$$\frac{dI_s}{dz} = g_R I_p I_s \tag{1.5}$$

Where I_s is the Stokes intensity, I_p is the pump intensity, and g_R is the Raman-gain coefficient. A similar relation holds for SBS with g_R replaced by the Brillouin-gain coefficient g_B. The Raman-gain spectrum is very broad, extending up to 30 THz [18].

An important feature of SRS and SBS is that they exhibit a threshold-like behavior, i.e. significant conversion of pump energy to Stokes energy occurs only when the pump intensity exceeds a certain threshold level. For SRS in a single-mode fiber with $\alpha L >> 1$, the threshold pump intensity is given by

$$I_p^{th} \sim 16(\alpha / g_R) \tag{1.6}$$

A similar calculation for SBS shows that the threshold pump intensity is given by [20]

$$I_p^{th} \sim 21(\alpha/g_B) \tag{1.7}$$

As the Brillouin-gain coefficient g_B is larger by nearly three orders of magnitude compared with g_R, typical values of SBS threshold are ~1 mW.

Importance of Nonlinear Effects

Most measurements of the nonlinear-index coefficient n_2 in silica fibers yield a value in the range $2.2 - 3.4 \times 10^{-20}\ m^2/W$, depending on both the core composition and whether the input polarization is preserved inside the fiber or not [19]. This value is small compared to most other nonlinear media by at least two orders of magnitude. Similarly, the measurements of Raman and Brillouin-gain coefficients in silica fibers show that their values are smaller by two orders of magnitude or more compared with other common nonlinear media [17]. In spite of the intrinsically small values of the nonlinear coefficients in fused silica, the nonlinear effects in optical fibers can be observed at relatively low power levels. This is possible because of two important characteristics of single-mode fibers—a small spot size (mode diameter < 10 μm) and extremely low loss (< 1 dB/km) in the wavelength range 1.0–1.6 μm.

A figure of merit for the efficiency of a nonlinear process in bulk media is the product IL_{eff} where I is the optical intensity and L_{eff} is the effective length of interaction region [10]. If light is focused to a spot of radiusW_0, then $I = P/(\pi W_0^2)$, where P is the incident optical power. Clearly, I can be increased by focusing the light tightly to reduceW_0. However, this results in a smaller L_{eff} because the length of the focal region decreases with tight focusing. For a Gaussian beam, $L_{eff} \sim \pi W_0^2/\lambda$, and the product

$$(IL_{eff})_{bulk} = \left(\frac{P}{\pi W_0^2}\right)\frac{\pi W_0^2}{\lambda} = \frac{P}{\lambda} \tag{1.8}$$

is independent of the spot size .In single-mode fibers, spot size W_0 is determined by the core radius a. Furthermore, because of dielectric wave guiding, the same spot size can be maintained across the entire fiber length L. In this case, the interaction length L_{eff} is limited by the fiber loss α.

1.3 Pulse-Propagation Equation

The study of most nonlinear effects in optical fibers involves the use of short pulses with widths ranging from _10 ns to 10 fs. When such optical pulses propagate inside a fiber, both dispersive and nonlinear effects influence their shape and spectrum. The basic equation that

governs propagation of optical pulses in nonlinear dispersive fibers can be derived from the equation:

$$\nabla^2 \boldsymbol{E} - \frac{1}{c^2}\frac{\partial^2 \boldsymbol{E}}{\partial t^2} = \mu_0 \frac{\partial^2 \boldsymbol{P}_L}{\partial t^2} + \mu_0 \frac{\partial^2 \boldsymbol{P}_{NL}}{\partial t^2} \tag{1.9}$$

Where the linear and nonlinear parts of the induced polarization are related to the electric field **E (r,** t**)**

Nonlinear Pulse Propagation

It is necessary to make several simplifying assumptions before solving the eq. above. First, is treated as a small perturbation to $\boldsymbol{P}_{NL}$. This is justified because nonlinear changes in the refractive index are < 10^{-6} in practice. Second, the optical field is assumed to maintain its polarization along the fiber length so that a scalar approach is valid. This is not really the case, unless polarization-maintaining fibers are used, but the approximation works quite well in practice. Third, the optical field is assumed to be quasi-monochromatic, i.e., the pulse spectrum, centered at ω 0, is assumed to have a spectral width Δω such that $\Delta\omega/\omega_0 \ll 1$. Since

ω_0 ~$10^{15} s^{-1}$, the last assumption is valid for pulses as short as 0.1 ps. In the slowly varying envelope approximation adopted here, it is useful to separate the rapidly varying part of the electric field by writing it in the form

$$\boldsymbol{P}_{NL}(\boldsymbol{r},t) = \varepsilon_0 x^{(3)} \; \boldsymbol{E}(\boldsymbol{r},t)\boldsymbol{E}(\boldsymbol{r},t)\boldsymbol{E}(\boldsymbol{r},t) \tag{1.10}$$

The assumption of instantaneous nonlinear response amounts to neglecting the contribution of molecular vibrations to $x^{(3)}$ (the Raman Effect). In general, both electrons and nuclei respond to the optical field in a nonlinear manner. The nuclei response is inherently slower compared with the electronic response. For silica fibers the vibrational or Raman response occurs over a time scale 60–70 fs. Thus, the eq. above is approximately valid for pulse widths of more than1 ps. In this $\boldsymbol{P}_{NL}$(**r**, t) is found to have a term oscillating at ω_0 and another term oscillating at the third-harmonic frequency $3\omega_0$. The latter term requires phase matching and is negligible in optical fibers. By making use of earlier equations, $\boldsymbol{P}_{NL}$(**r**, t) is given by

$$\boldsymbol{P}_{NL}(\boldsymbol{r},t) \approx \boldsymbol{\varepsilon_0 \varepsilon_{NL} E}(\boldsymbol{r},t) \tag{1.11}$$

CHAPTER 2

SOLITON PROPAGATION IN OPTICAL FIBERS

2.1 Introduction

In this chapter, we study soliton propagation in optical fibers. A numerical model will be developed to describe the soliton propagation. The nonlinear Schrödinger equation (NLSE), modified to include cubic dispersion, self-steepening, and stimulated Raman scattering, will be solved numerically using the Split-Step Fourier Method (SSFM).

Numerical results will be presented for N=1, N=2, and N=3 soliton propagation.

2.2 Numerical Analysis

The nonlinear Schrodinger equation (NLSE) is a basic equation for the description of pulse propagation in optical fibers that are nonlinear and dispersive. The NLSE can be derived from the wave equation after the effects of the nonlinearity and dispersion are included under the slowly-varying envelope approximation. The derivation of the NLSE from wave equation can be found in the reference [12]. The resulting NLSE modified to include higher-order effects. This equation is valid for describing the propagation of pulses as short as ~ 50 fs.

The last three terms embody the higher-order effects; they are, respectively, cubic dispersion, self-steepening, and stimulated Raman scattering. The effect of cubic dispersion becomes important for ultra short pulses, whose bandwidths are large. Under such conditions, cubic dispersion is important even when the wavelength λ is relatively far away from the zero-dispersion wavelength λ_0 [13]-[14]. The effect of self-steepening is responsible for shock formation at a pulse edge [15]-[17]. The last term, proportional to *TR*, results from Stimulated Raman scattering, and is responsible for the self-frequency shift, which transfers energy from shorter-wavelengths to longer-wavelengths.

It is convenient to use normalized dimensionless units by using the definitions The cubic dispersion, self-steepening, and Raman response parameters *Aeff* is the effective area of the fiber mode intensity, and $D(\lambda)$ is the quadratic dispersion in ps/nm-km. *N* provides a measure of the strength of the nonlinear response compared to the fiber dispersion. Not only the initial pulse width *T0* and the peak power *P0* of the incident pulse, but also the fiber parameters *n2*, *Aeff*, and *D* can change the soliton order *N*. The effects of δ, s, and τ R are described in detail later. To minimize their contributions, pulses must be sufficiently broad to enable modest peak powers and longer rise and fall times, while satisfying the higher order soliton condition. Consequently, we are constrained to input pulses of widths *T0*>1ps such that *T0* ω *0*>>1 and *TR/T0*<<1, at which δ, s, and τ R can be negligible [19]. For pulse widths of the order of 1 ps or longer, Equation (2.2.8) is referred to as the NLSE and has been extensively studied in the context of solitons, which are its solutions. Optical solitons can exist through balance and interplay between the dispersive (GVD) and nonlinear (SPM) properties of optical fibers.

Fundamental solitons correspond to the case of a single eigen value (N=1). They can propagate over arbitrarily long distances, maintaining their shapes and widths in time and in the spectral domain. Fundamental solitons are a good candidate for high-speed data transmission systems because they can easily overcome GVD induced pulse broadening.

Higher-order solitons are the general solutions of the NLSE for integer values of N greater than 1. Instead of propagation without changing shape, they show periodic propagation behavior in their shapes and widths over the soliton period.

Higher-order solitons have found applications to optical pulse compression. To investigate soliton propagation in optical fibers, we numerically solved Equation (2.2.8) using the Split-step Fourier method, which will be introduced in the next section.

2.3 Numerical Method: Split-step Fourier Method

The operator $\hat{D}$ includes the effects of dispersion in a linear medium, whereas the operator $\hat{N}$ includes the effects of fiber nonlinearities on pulse propagation. During the pulse propagation, dispersion and nonlinearity act together. This makes the numerical solution complicated. Under some assumption that dispersion and nonlinearity can act independently during the propagation of the optical field over a small distance, the numerical solution can be easily obtained. The split-step Fourier method adopts this assumption for the independent actions of GVD and SPM to obtain an approximate numerical solution. For example, propagation from z to z+h is carried out in two steps. In the first step, only nonlinearity is considered by setting $\hat{D}=0$. In the second step, only dispersion is considered by setting $\hat{N}=0$.

FIGURE 2.1 shows an operation diagram of the symmetrized split-step Fourier method used for numerical simulations. The propagation path is partitioned into a number of segments. The step size *h* should be small enough to satisfy the accuracy requirement for the approximation. As the step size decreases, accuracy increases but computation time is also increases. First, GVD acts alone in frequency domain without SPM between the input and the center of each segment. At the center of the segment, SPM is considered in time domain without GVD. Then GVD acts alone again in frequency domain without SPM through the remaining half of the segment. This process is repeated until all segments are completed.

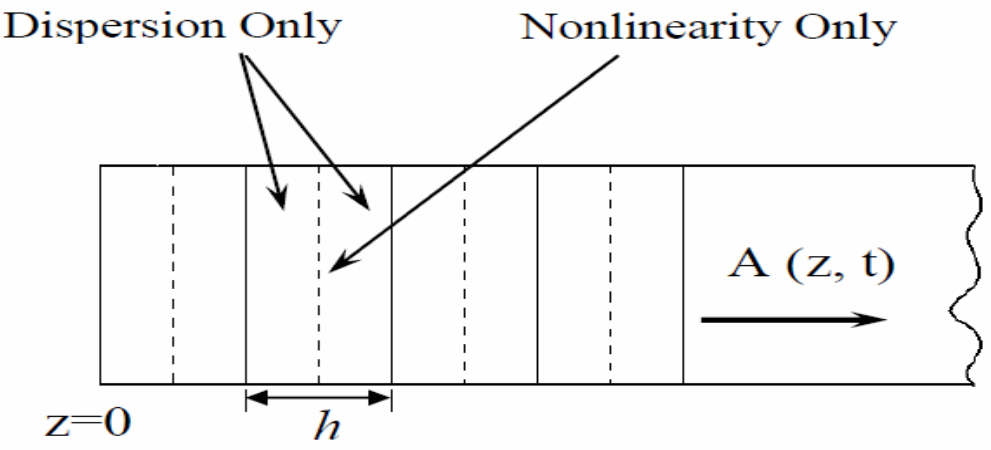

FIGURE 2.1 Diagram of the split-step Fourier method used for numerical simulations.

2.4 Numerical Results

To investigate soliton propagation in optical fibers, we numerically solved the NLSE using Split-step Fourier method with the initial envelope of the soliton at $\xi = 0$ given by $U(0, \tau)=\text{sech}(\tau)$ for N=1, N=2, and N=3 cases.

2.4.1 Fundamental soliton propagation (N=1)

Figures 2.2a and b show the temporal and spectral evolution of a fundamental soliton over one soliton period *z0*, It shows that the soliton can propagate with an unchanging pulse envelope and its spectrum over long distances. This can be achieved through the balance between the effects of SPM and GVD.

The physical process of fundamental soliton propagation can be explained by considering the effects of SPM and GVD. During the pulse evolution, the effect of SPM is to produce positive chirp, whereas the effect of GVD (D>0) is to produce negative chirp. When relative strengths of SPM and GVD are exactly balanced, positive chirp generated by SPM is completely cancelled out by negative chirp generated by GVD. As a result, the pulse exhibits a zero chirp with time over its entire width. Under this condition, the pulse propagates without broadening or compressing for long distances.

The soliton order, N, is an indicator of nonlinear strength, which means the ratio of the strength of nonlinear effect to that of dispersion effect. For fundamental solitons (N=1), the effects of SPM and GVD are exactly balanced.

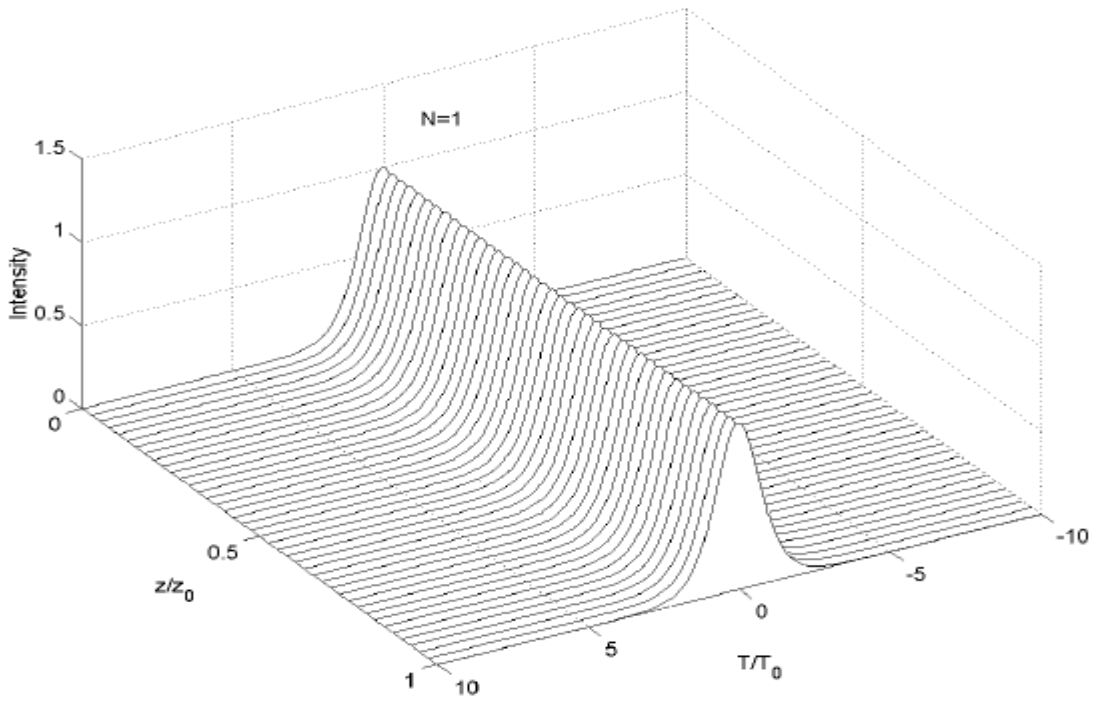

FIGURE 2.2a Temporal evolution of an N=1 soliton over one soliton period, *z0*. The intensity is normalized to the input peak intensity.

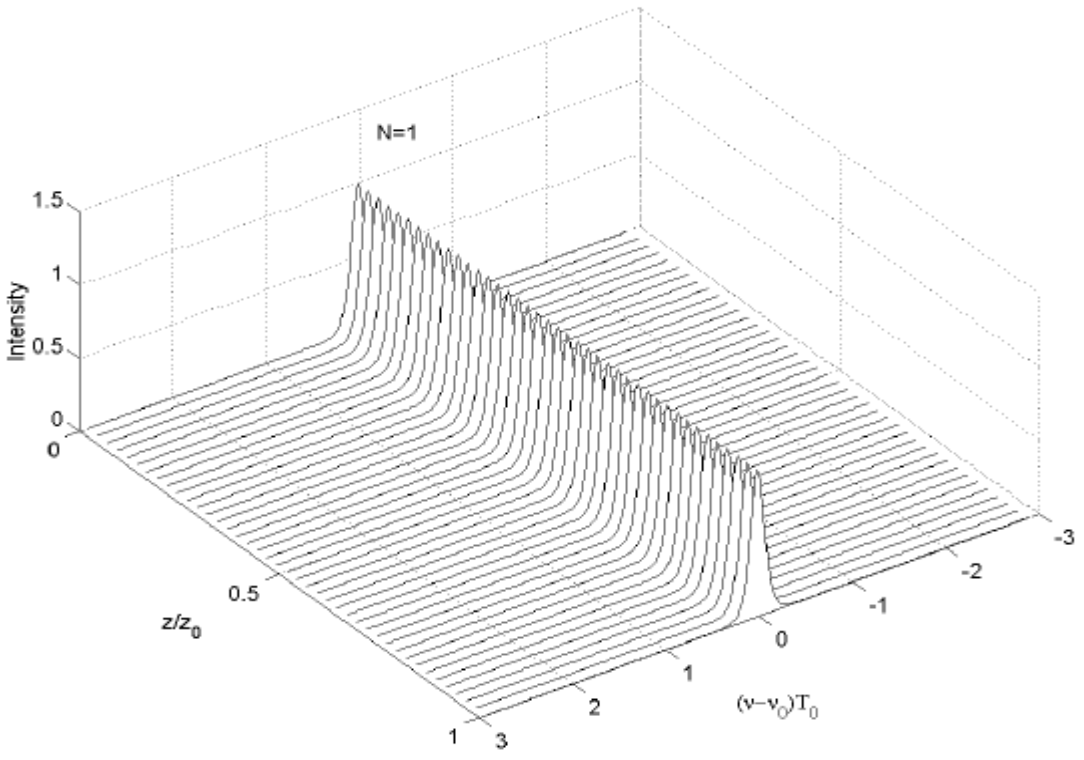

FIGURE 2.2b Spectral evolution of an N=1 soliton over one soliton period, *z0*. The intensity is normalized to the input peak intensity.

2.4.2 Second-order soliton propagation (N=2)

If *N* is an integer greater than 1, pulse evolution is totally different from the case of a fundamental soliton. Evolution of this *N*th-order soliton is periodic. For higher-order solitons, the effect of SPM dominates the effect of GVD (N>1). As discussed in the previous section, the effect of SPM is to produce positive chirp, whereas the effect of GVD (D>0) is to produce negative chirp. Because of the higher intensity, the amount of positive chirp generated by SPM is greater than that of negative chirp produced by GVD; it cannot be cancelled out completely. As a result, the pulse acquires positive chirp.

The effect of GVD (D>0) for a positively chirped pulse is to compress the pulse by forcing the energies associated with its spectral components toward the center. With SPM of greater magnitude than in the N =1 case, the pulse would compress until the energies reach the center. As they pass through the center, the pulse will broaden again.

The temporal and spectral evolution of an N =2 soliton are shown in Figures 2.3a and b. In time domain, the pulse compresses up to the distance z0/2, at which it has a minimum pulse width. This pulse compression occurs because N is greater than 1. The amount of positive chirp from SPM is too large to be canceled by negative chirp generated from GVD. As a result, it is accumulated and is increased up to the distance z0/2, where the shifted energies by positive dispersion coincide at the pulse center. As soon as they pass through the center, the sign of chirp is changed from positive to negative. The effect of GVD (D>0) for a negatively chirped-pulse is to broaden the pulse.

After the distance z0/2, the pulse begins to re-broaden. Because positive chirp generated by SPM rapidly cancels the negative chirp on the pulse, the amount of negative chirp is decreased and pulse spreading slows down. The chirp becomes zero at the distance z0, where the pulse stabilizes at its original width. The process then repeats.

In spectral domain, the pulse spectrum broadens as the pulse compression occurs. At the distance z0/2, the spectrum splits to form two peaks. This can be interpreted as two overlapping pulses at the two wavelengths in time domain. After the distance z0/2, the separated spectral peaks recombine as the pulse propagates. Then the spectrum is recompressed to recover the original input spectrum.

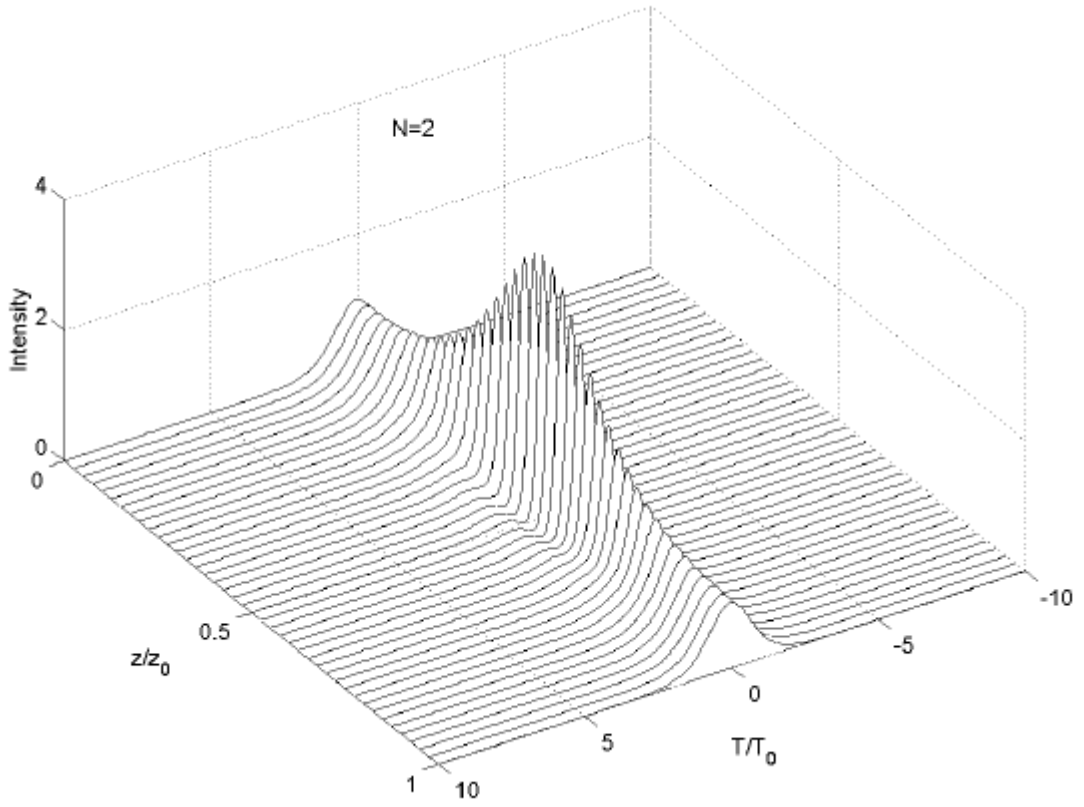

FIGURE 2.3a Temporal evolution of an N=2 soliton over one soliton period, *z0*. The intensity is normalized to the input peak intensity.

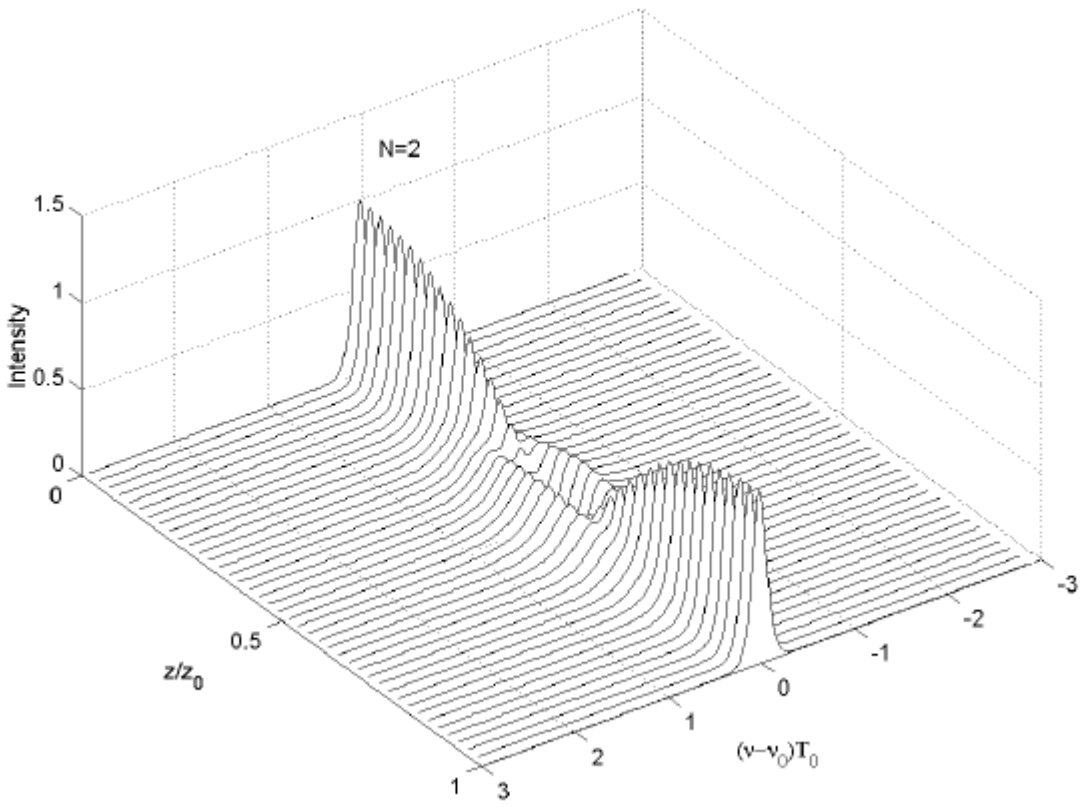

FIGURE 2.3b Spectral evolution of an N=2 soliton over one soliton period, *z0*. The intensity is normalized to the input peak intensity.

2.4.3 Third-order soliton propagation (N=3)

Higher-order solitons show more complicated SPM-GVD interplay as the soliton order increases. Figure 2.4a and 2.4b show temporal and spectral evolution of N=3 soliton over one soliton period. The evolution is symmetric about *z0*/2 and is repeated every z0. At the initial stage of evolution, the pulse contracts with increasing intensity. It then splits into a two-peaked pulse near *z0*/2. After z = *z0*/2, pulse undergoes the reverse process. It merges again and recovers its initial shape.

Figure 2.5 shows the temporal shape, phase, chirp, and spectrum during N =3 evolution over one soliton period. In the initial stage of evolution (up to *z*/*z0* = 0.25), pulse compression is a dominant property. SPM generates positive chirp. Therefore the pulse contracts like a positively pre-chirped pulse in anomalous GVD region. Since the positive chirp is linear near over the pulse center, only this part of the pulse can contract.

The rest of the pulse has negative chirp, so this portion becomes disperses and forms side lobes like a pulse shape at *z*/*z0* = 0.25 in Figure 2.5. The pulse intensity has its maximum at around *z*/*z0* = 0.25. The pulse spectrum of the initial stage shows the typical SPM induced spectral broadening, clearly seen at *z*/*z0* = 0.25. Between 0.20 *z0* and 0.25 *z0*, the energies at the offset frequencies pass through the pulse center. In Figure 2.5, the peak phase at z/z0 = 0.20 has reached π radians and thereafter flips to $-\pi$, as shown in the phase plot at *z*/*z0* = 0.25. As a result, negative chirp appears across over the pulse center, as shown in the corresponding $\delta\ \omega$ plots. The pulse now begins to re-broaden as result of having negative chirp within the anomalous GVD region. Then the pulse begins to split apart at *z*/*z0* = 0.35, at which there are two regions of positive chirp on either side of a region of negative chirp, as shown in the $\delta\ \omega$ plot. With positive dispersion (D>0), the positively-chirped region of the pulse will be compressed, while the negatively-chirped region of the pulse will be broadened. This leads to a splitting of the pulse in time domain, as shown in the shape plot at *z*/*z0* = 0.40. After 0.5z0 the pulse evolution is exactly the reverse process. Chirp is completely anti-symmetric about 0 0.5*z* . Since GVD is a linear process, the pulse shape can be recovered.

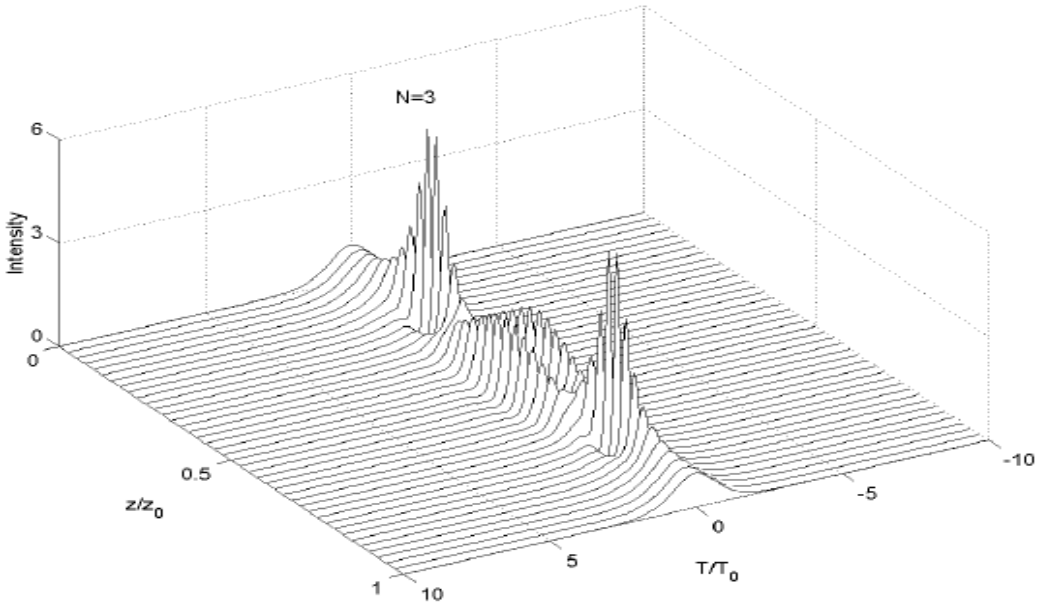

FIGURE 2.4a Temporal evolution of an N=3 soliton over one soliton period, *z0*. The intensity is normalized to the input peak intensity.

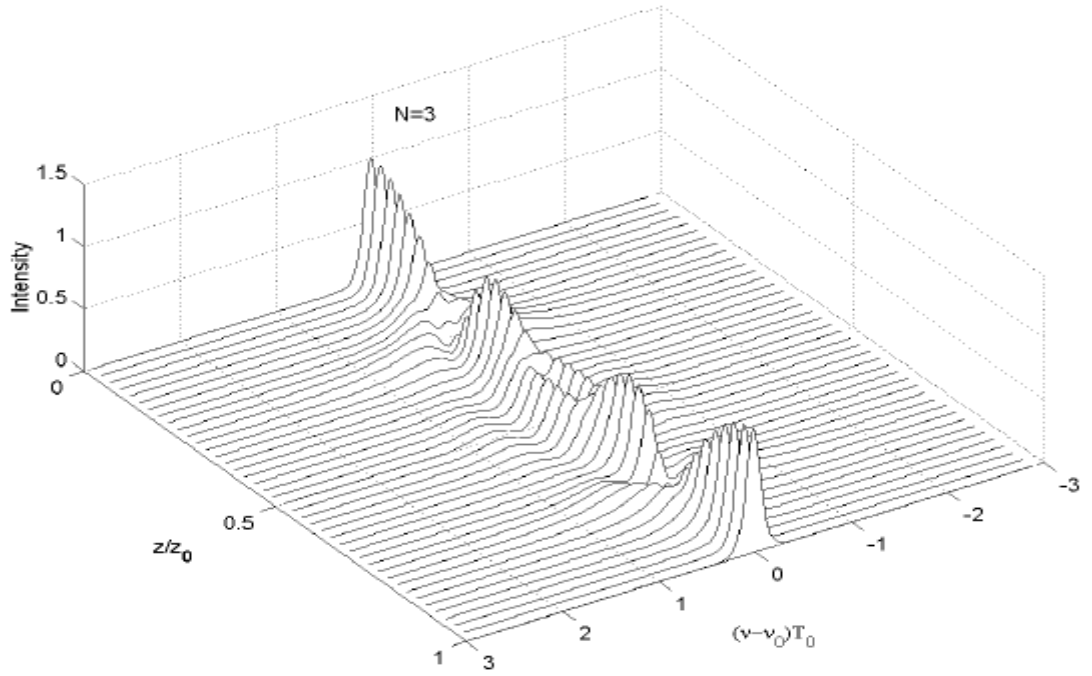

FIGURE 2.4b Spectral evolution of an N=3 soliton over one soliton period, *z0*. The intensity is normalized to the input peak intensity.

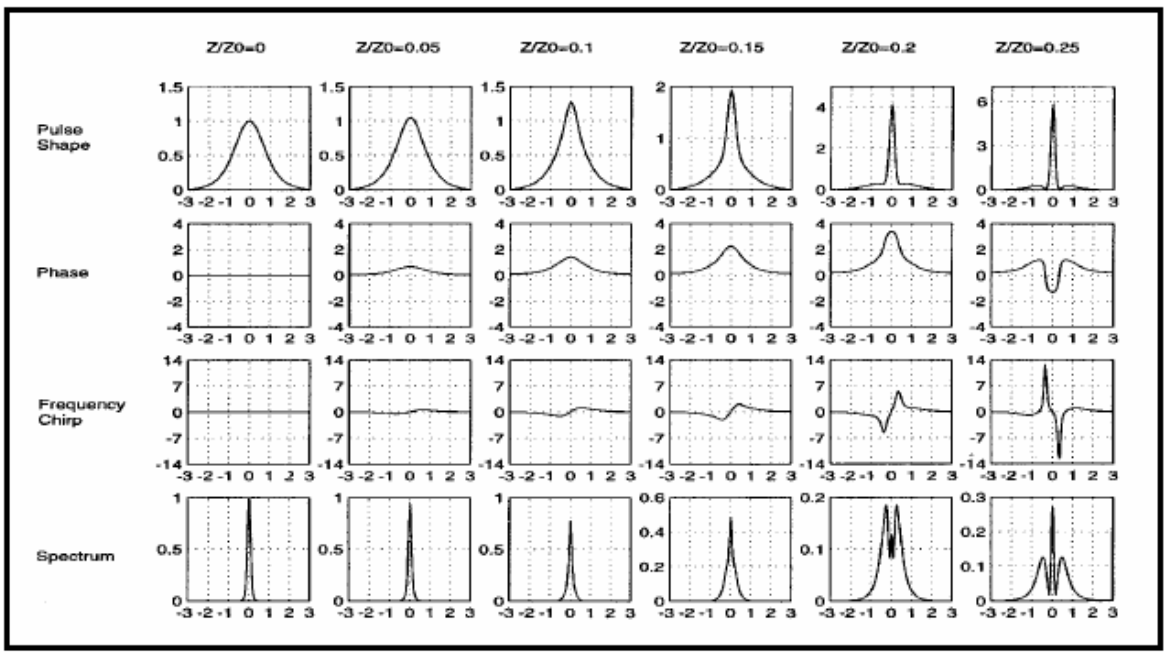

FIGURE 2.5 (with the following three pages) Soliton temporal envelope, nonlinear phase shift, frequency chirp, and pulse spectrum of an N=3 soliton over one soliton period, *z0*.

CHAPTER 3

HIGHER-ORDER SOLTON DECAY

3.1 Introduction

In this chapter, we study the decay of higher order solitons in optical fibers. The decay of higher order solitons initiated by localized channel perturbations in the fiber will be proposed to obtain tunable wavelength separation. The perturbation is applied using a step change in dispersion, a loss element, or a bandpass filter. All result in the conversion of the soliton into two sub-pulses at wavelengths that are up and down-shifted from that of the input pulse. The wavelengths can be varied by adjusting the magnitude of the perturbation. Pulse parameter requirements for achieving useful wavelength shifts while avoiding unwanted nonlinear effects are presented. In principle, the converted pulses can be amplified to form separate higher order solitons, and the process repeated to produce multiple wavelengths of variable spacing; care is required, however, to assure that detrimental effects associated with amplification, such as amplified spontaneous emission (ASE), are avoided [20].

3.2 Physical Perspective

Our studies center on the response of solitons of order N=2 or N=3 to the aforementioned three perturbations. As diagramed in Figure 3.1, during the unperturbed evolution of these solitons with distance, wavelength spectra broaden and separate into two peaks (for N=2) or three peaks (for N=3), where in the latter case, the original center wavelength is retained. The maximum spectral separation, $\Delta \lambda_{max}$, occurs at locations corresponding to 0.5 $z0$ for N=2 and 0.25 $z0$ for N=3. As is well-known, further propagation results in the spectra re-compressing to form the original input. The process repeats, completing the cycle each soliton period distance, $z0$. While spectra are separated, the soliton in time domain can be thought of as two or three overlapping pulses that are associated with the separated spectral components.

Figure 3.2 and Figure 3.3 show our soliton decay methods for N=2 and N=3 solitons respectively. Our method involves placing the perturbations at the $\Delta\lambda_{max}$ locations, where the maximum spectral separation occurs, corresponding to 0.5 *z0* for N=2 and 0.25 *z0* for N=3 (see Figure 3.1). By doing so, the nonlinear response of the fiber beyond the perturbation is effectively reduced, thus preventing the complete return of the spectrum to its original form. The composite pulses, retaining their individual spectra, separate in time owing to their different group velocities. The reduced nonlinear response beyond the perturbation then participates in the continued evolution of the separated pulses in the following ways: 1) the sub-pulses may evolve into fundamental solitons or nearly so — i.e., into pulses that exhibit little change over several dispersion distances; 2) the spectrum partially re-compresses, leading to a wavelength spacing between sub pulses that is less than the value just before the perturbation. Consequently, by varying the magnitude of the perturbation (equivalent to varying the nonlinear strength in the channel beyond the perturbation), the wavelength spacing between the sub-pulses, $\Delta\lambda$, can be varied.

Maximum wavelength spacings obtainable for N=2 and N=3, as a functions of FWHM input pulse width, are plotted in Figure 3.4 for a 1.55 μm center wavelength. As an example, if a 10 ps pulse is used, a maximum spacing for N=2 of $\Delta\lambda_{max}$=0.8nm (100 GHz) can be obtained by using a large perturbation at the 0.5 *z0* position. The wavelength spacing can be reduced from this value by weakening the perturbation. If an N=2 soliton is used, only the shifted wavelengths remain in the signal. For an N=3 soliton, sub-pulses are generated that can have a larger wavelength spacing than those in an N=2 pulse, and a relatively weak pulse at the original carrier wavelength remains.

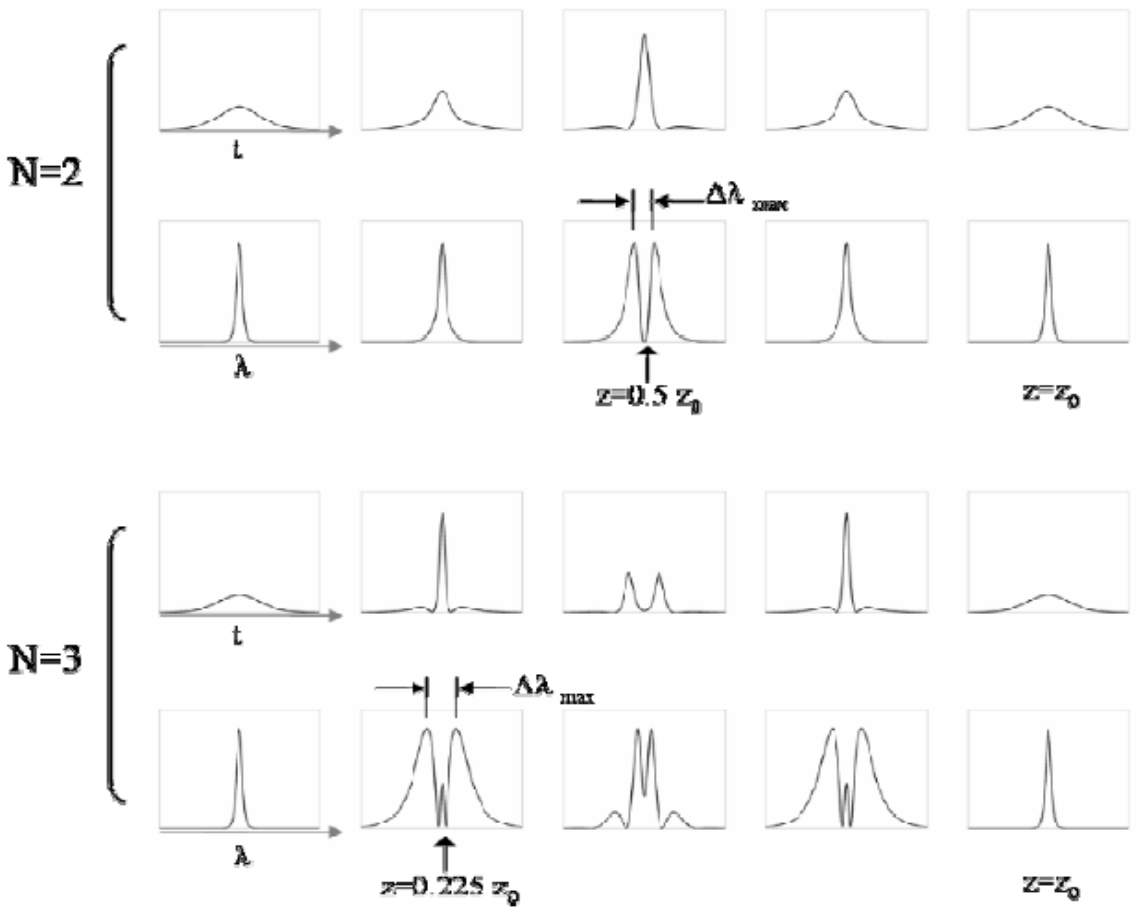

FIGURE 3.1 Temporal and spectral evolution of unperturbed N=2 and N=3 solitons at selected positions in the fiber channel. Perturbation locations used in this work are indicated.

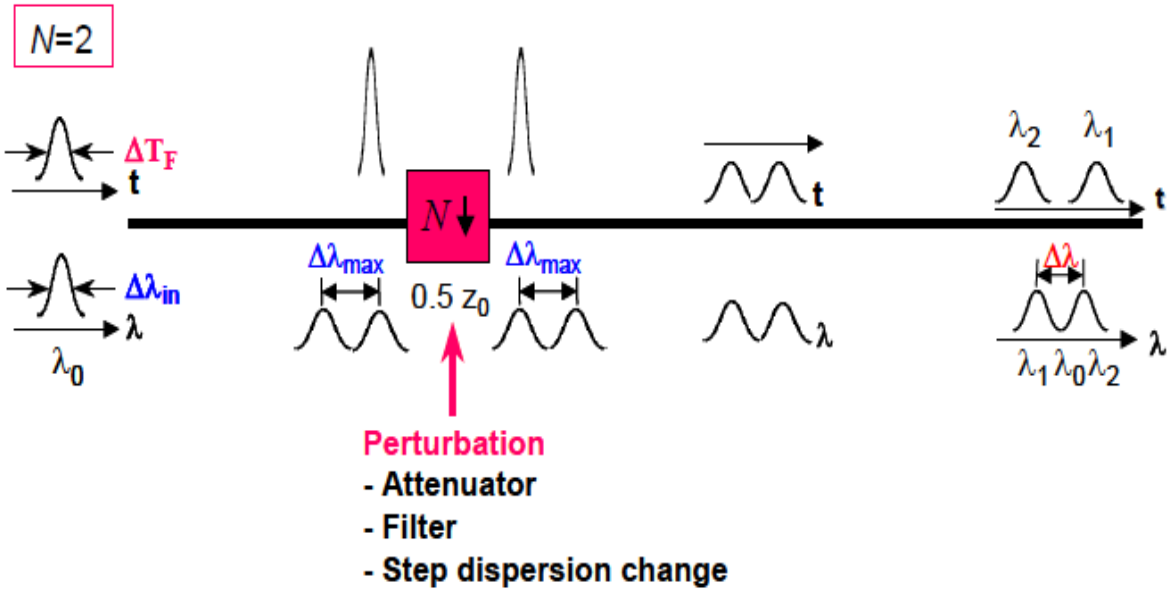

FIGURE 3.2 Temporal separation of the N=2 soliton spectral components as a result of a perturbation applied at the half soliton period distance. The perturbation reduces the value of the soliton number, N, and so only partial spectral re-compression occurs. Fundamental solitons at the separated wavelengths may evolve if a dispersion step perturbation is used.

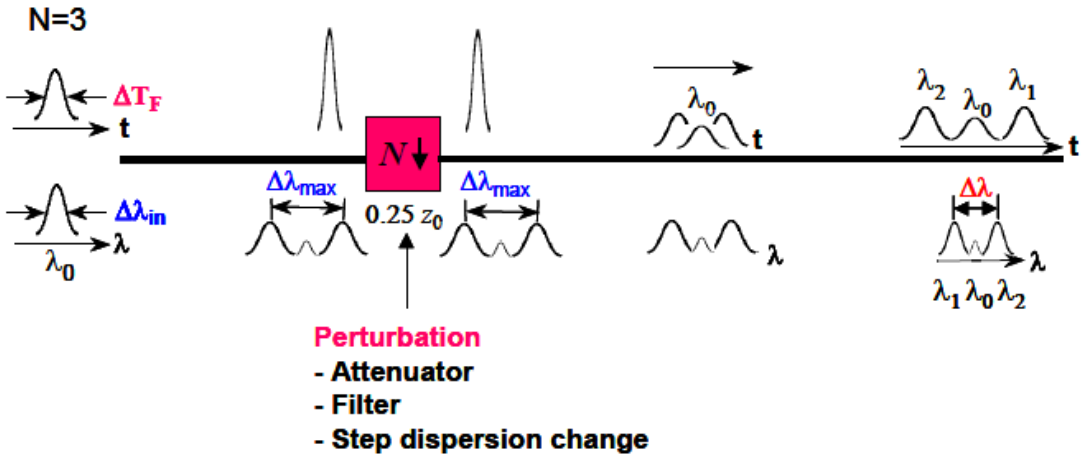

FIGURE 3.3 Temporal separation of the N=3 soliton spectral components as a result of a perturbation applied at the half soliton period distance. The perturbation reduces

the value of the soliton number, N, and so only partial spectral re-compression occurs. Fundamental solitons at the separated wavelengths may evolve if a dispersion step perturbation is used.

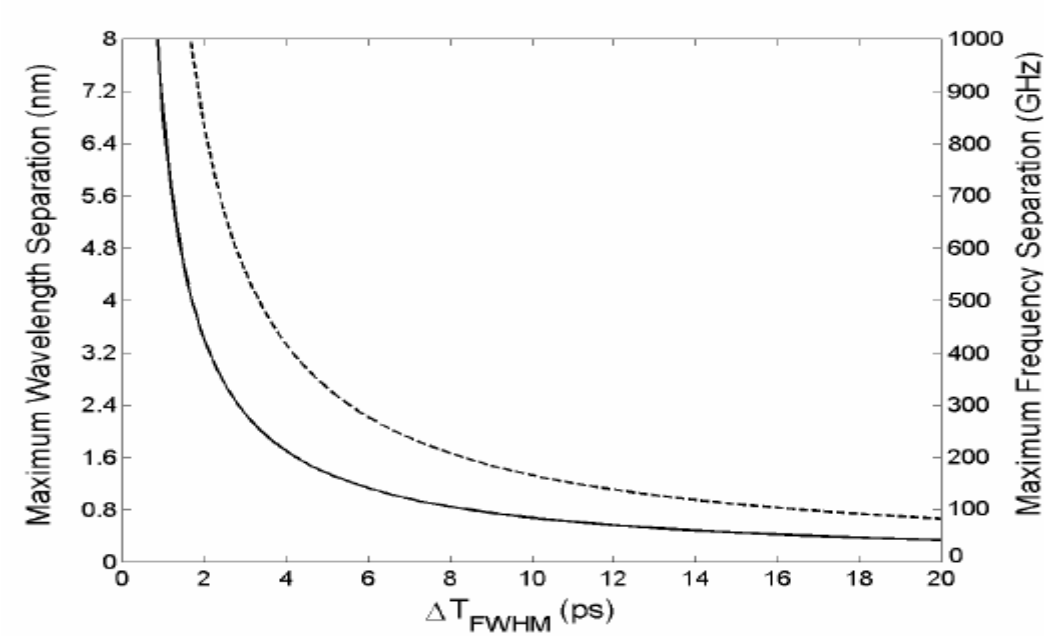

FIGURE 3.4 Maximum obtainable wavelength separations $\Delta\lambda_{max}$ as functions of input pulse width for N=2 (solid curve) and N=3 (dashed curve) solitons. The corresponding frequency separations at 1.55 μm wavelength are indicated on the right vertical axis.

3.3 Numerical Results

To investigate the soliton decay, we solved the equation (2.2.6) given by:

$$\frac{\partial U}{\partial z} - \frac{i}{2}\frac{\partial^2 U}{\partial \tau^2} - \delta\frac{\partial^3 U}{\partial \tau^3} = iN^2\left[|U|^2 U + is\frac{\partial}{\partial \tau}(|U|^2 U) - \tau_R U\frac{\partial}{\partial \tau}(|U|^2)\right].$$

As described in Section 2.2, U is the normalized complex envelope of the pulse, ξ is the normalized distance, and τ is the normalized local time. The cubic dispersion,

self steepening, and Raman response parameters are respectively given by $\delta = \beta 3/(6|\beta 2|T0)$, s=1/(T0 ω 0), and τ R=TR/ T0. The initial envelope of the soliton at ξ = 0 is given by U(0, τ)=sech(τ).

The soliton order, N, in the above equation provides a measure of the strength of the nonlinear response, compared to the fiber dispersion. Applying the perturbation effectively reduces the value of N for all positions at and beyond the point of application.

From (2.2.7), it is seen for example that N is decreased by increasing D or by decreasing P0, the latter being accomplished in our case by a loss element or a band pass filter. With the perturbation applied, the separated pulses may evolve into fundamental solitons, provided energy is not removed from the pulse pair. A step increase in dispersion will satisfy this requirement, whereas a loss element or filter will not. The effects of δ , s, and τ R are described in detail later. To minimize their contributions, pulses must be sufficiently broad to enable modest peak powers and longer rise and fall times, while satisfying the higher order soliton condition. Consequently, we are constrained to input pulses of widths T0>1ps such that T0 ω 0>>1 and TR/T0<<1, at which δ , s, and τ R can be negligible [19]. Under this constraint, but nevertheless including all higher order terms, the NLSE was solved using the split-step Fourier method, in which a reduction in pulse amplitude or bandwidth, or an increase in fiber dispersion was incorporated at the maximum bandwidth positions.

Figure 3.5 shows the separation of ΔTf =1 ps sub-pulses originating in an N=2 soliton after a step increase in dispersion at the *z0*/2 location. Using a transition to higher dispersion fiber effectively reduces the value of N, while maintaining the pulse energy, thus enabling the sub-pulses to evolve into fundamental solitons. In this example, the initial dispersion is 8 ps/nm-km (for z=0 to 0.5z0) and is step-increased to 16 ps/nm-km (for z=0.5z0 to 2.5z0). As shown in Figure 3.5, the separation between the two pulses increases linearly with the distance, indicating group velocity differences arising from their having different center wavelengths. This is confirmed

by the spectrum (Figure 3.5a inset). Increasing the run time, allowing further propagation over several dispersion lengths yielded no discernable change in pulse shape or width.

Sub-pulse formation from N =3 solitons using the same dispersion change as in Figure 3.5 are shown in Figure 3.6, except the position of the dispersion step is at z=0.225 z0. In this case, the original soliton decays into two sub-pulses at the shifted wavelengths, with a remnant of the original carrier wavelength surviving as a third weaker pulse. The spectral separation between pulses is greater than that in the N=2 case, and again, no discernable change in the wavelength-translated pulses was found after propagating through several dispersion lengths. The plots in Figure 3.5 show results under lossless propagation. When including fiber loss of 0.2 dB/km, the effect is negligible for pulse widths on the order of 1 ps. With longer pulses, the dispersion length (proportional to the square of the pulse width) may be sufficiently long to affect the pulse energy during the evolution process. The effects are 1) a longer distance is needed to achieve $\Delta \lambda max$ (for example 0.55z0 instead of 0.5 z0 for a 10 ps N=2 input), and 2) the expected power reduction with distance of the output fundamental solitons occurs, along with their eventual dissipation.

As an alternative to a dispersion step, use of an attenuator or a filter reduces the nonlinear response beyond the perturbation by removing energy from the pulse. Figure 3.7 and 3.8 show the separation of ΔTf =1 ps sub-pulses originating in an N=2 soliton after 3dB attenuation and bandbass filtering at the *z0*/2 location respectively. The transformed pulses appear similar to those shown in Figure 3.5, but decay asymptotically to eventually dissipate. Nevertheless, they were found to exhibit almost chirp-free fundamental soliton behavior over several dispersion lengths, even when distributed losses were included.

Wavelength spacings between sub-pulses as functions of the dispersion difference, attenuation, and filter bandwidth ($\Delta \lambda$ f) of the channel perturbation are plotted in Figure 3.9 for N=2 and N=3. In Figure 3.9, the wavelength spacing and the filter width are normalized with respect to the input spectral width $\Delta \lambda$ in (in turn inversely

proportional to the input pulse width). The bandpass filter has a Gaussian shape, and is centered at the input pulse carrier frequency. When a dispersion step or an attenuator is used, the wavelength separation increases toward the maximum allowable value (as can be determined from Figure 3.4) as the perturbation magnitude increases. For example, wavelength spacings from 0 to 10 nm are predicted for a 1ps input pulse by changing dispersion between 10-80% or by attenuating the signal between 1 and 5 dB. On the other hand, when using a filter, the perturbation magnitude increases with decreasing filter width. The curves in Figure 3.9c are seen to reach local maxima, and then fall off as the filter width becomes narrower. This would be expected, since the filter itself would eventually block transmission of the more widely-spaced spectral components.

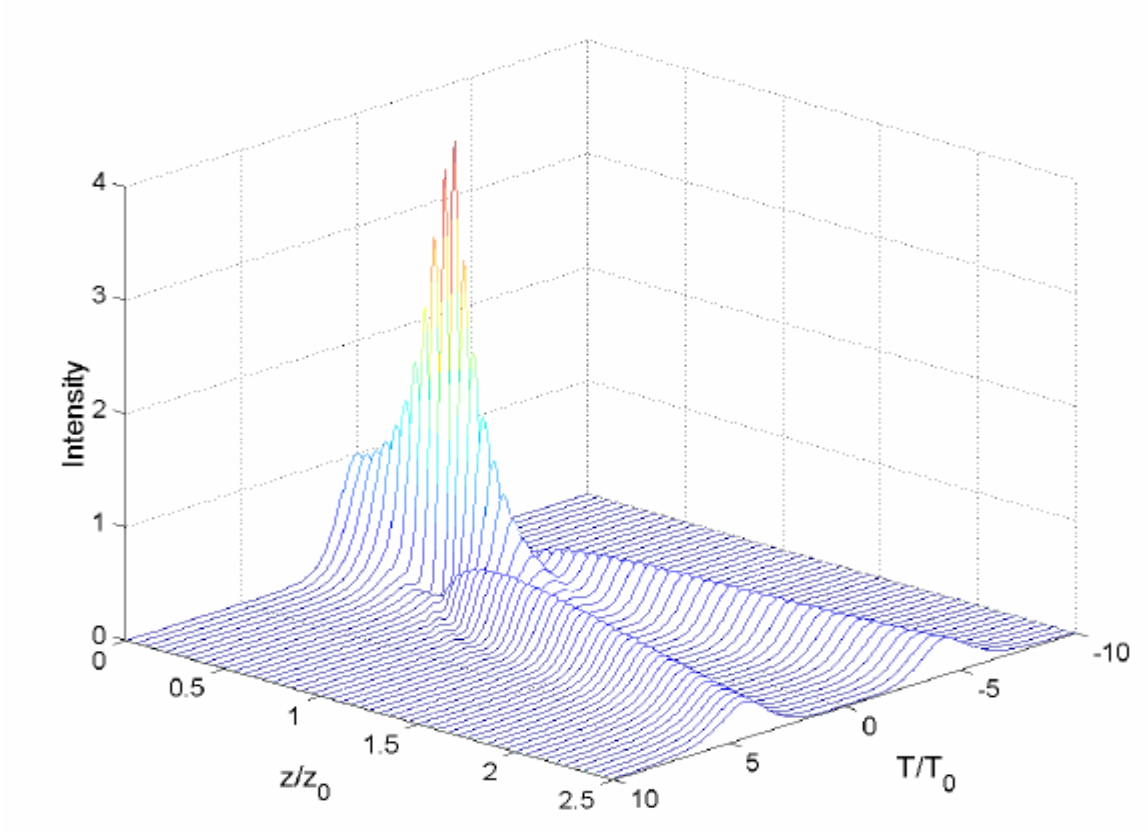

FIGURE 3.5 Numerical results, showing the decay of an N=2 soliton, initiated by a step increasing the dispersion from 8 ps/nm-km to 16 ps/nm-km at the position, $z/z_0=0.5$. Temporal (a) and spectral (b) evolution on next page show the formation of nearly fundamental solitons at two wavelengths.

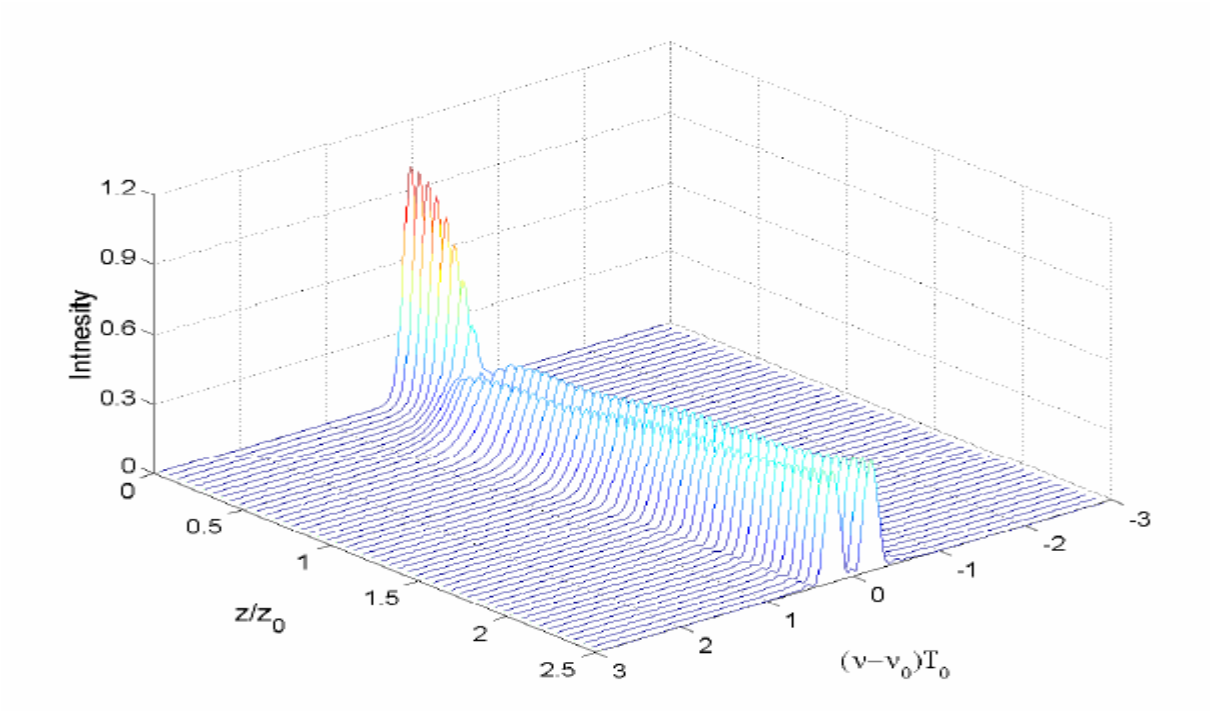
Intnesity
1.2
0.9
0.6
0.3
0
0
0.5
1
1.5
2
2.5
z/z0
3
2
1
0
-1
-2
-3
(ν−ν0)T0

(b)

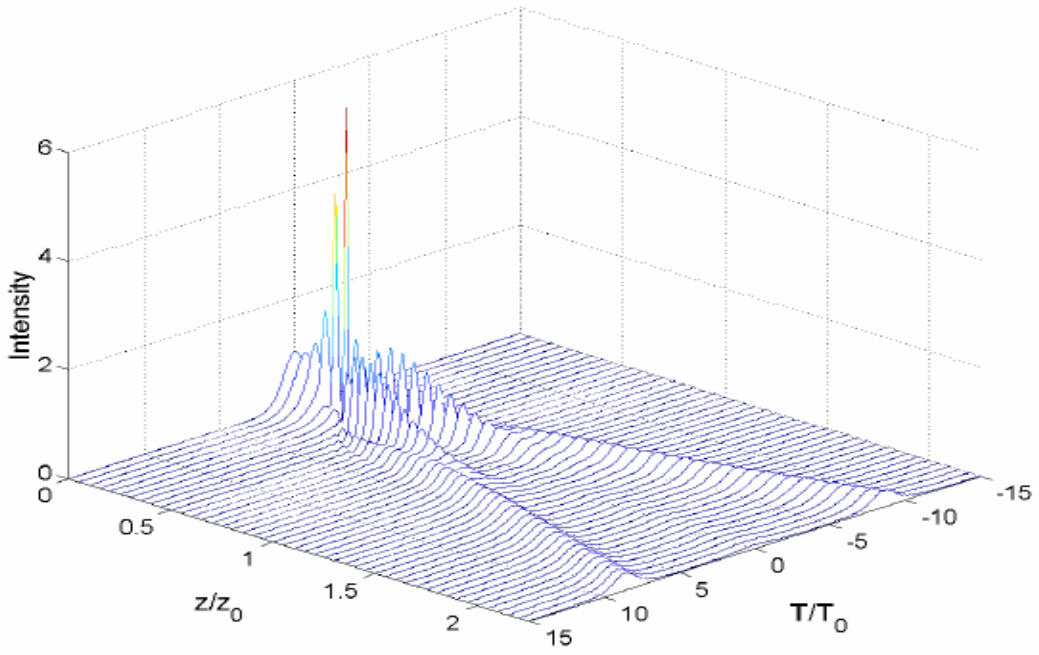
Intensity
6
4
2
0
0
0.5
1
1.5
2
z/z0
15
10
5
0
-5
-10
-15
T/T0

(a)

FIGURE 3.6 Numerical results, showing the decay of an N=3 soliton, initiated by a step increasing the dispersion from 8 ps/nm-km to 16 ps/nm-km at the position, z/z0=0.25. Temporal (a) and spectral (b) evolution on next page show the formation of nearly fundamental solitons at three wavelengths.

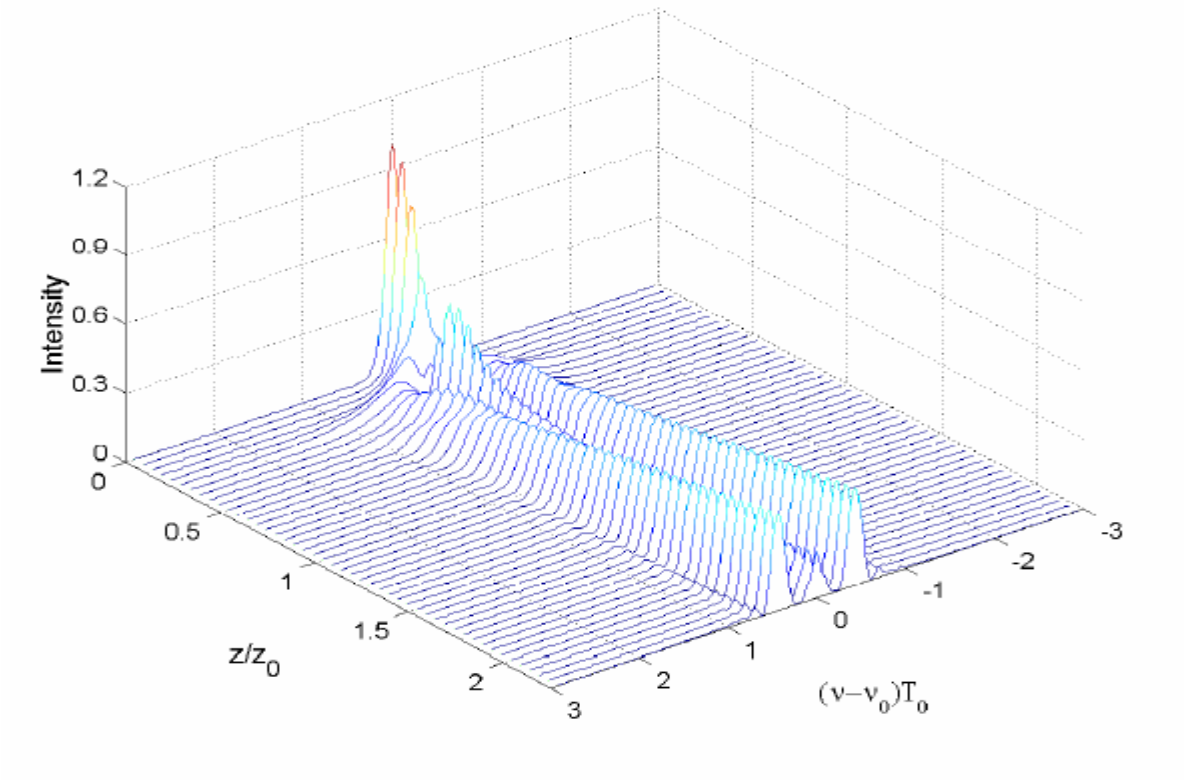

(b)

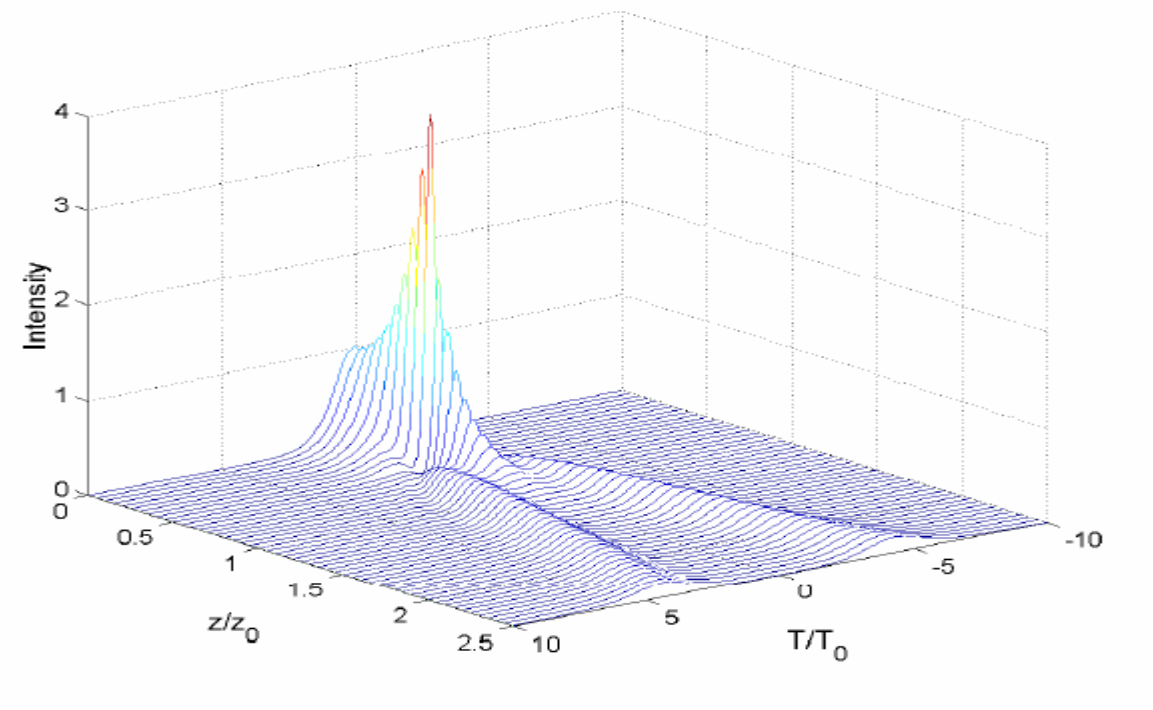

(a)

FIGURE 3.7 Numerical results, showing the decay of an N=2 soliton, initiated by attenuation (3dB) at the position, z/z0=0.5. Temporal (a) and spectral (b) evolution shows the formation of sub pulses at two wavelengths.

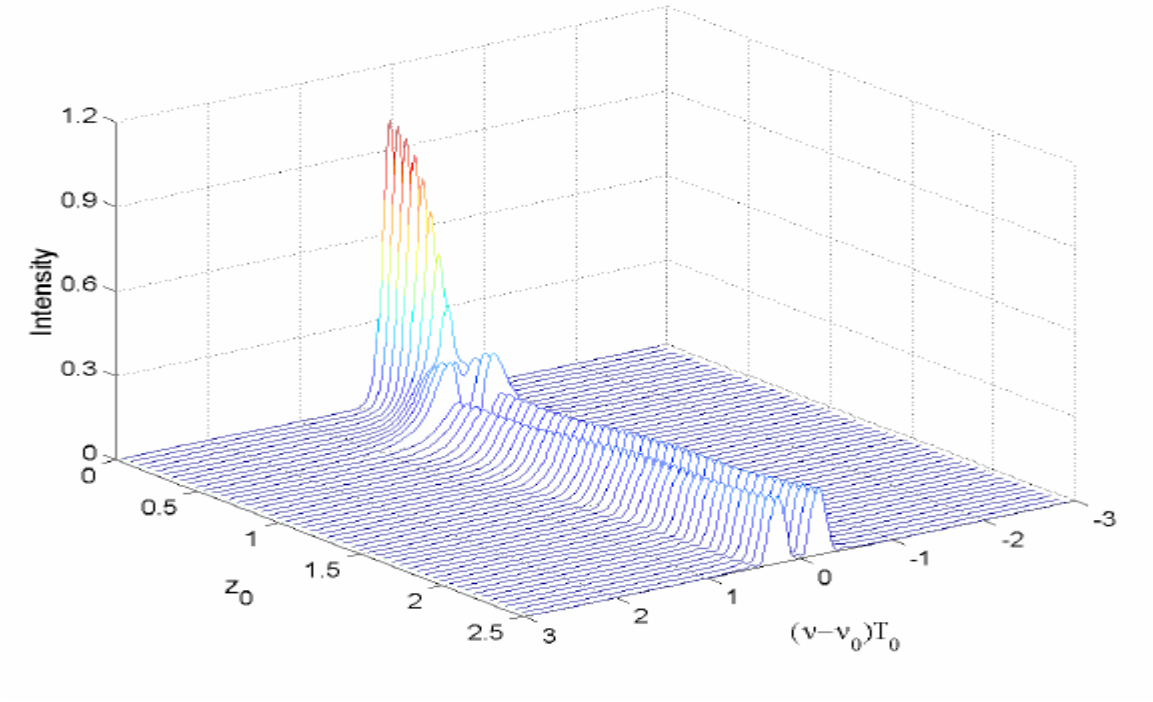

(b)

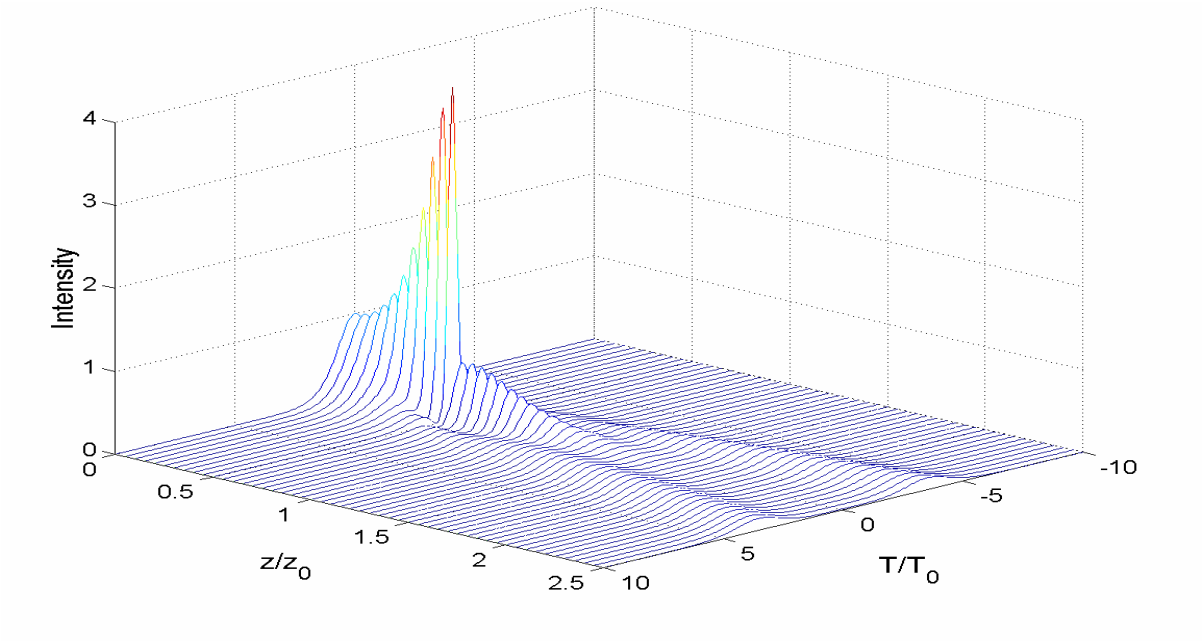

(a)

FIGURE 3.8 Numerical results, showing the decay of an N=2 soliton, initiated by bandpass filtering ($\Delta \lambda f / \Delta \lambda in = 2.72$) at the position, z/z0=0.5. (a) Temporal

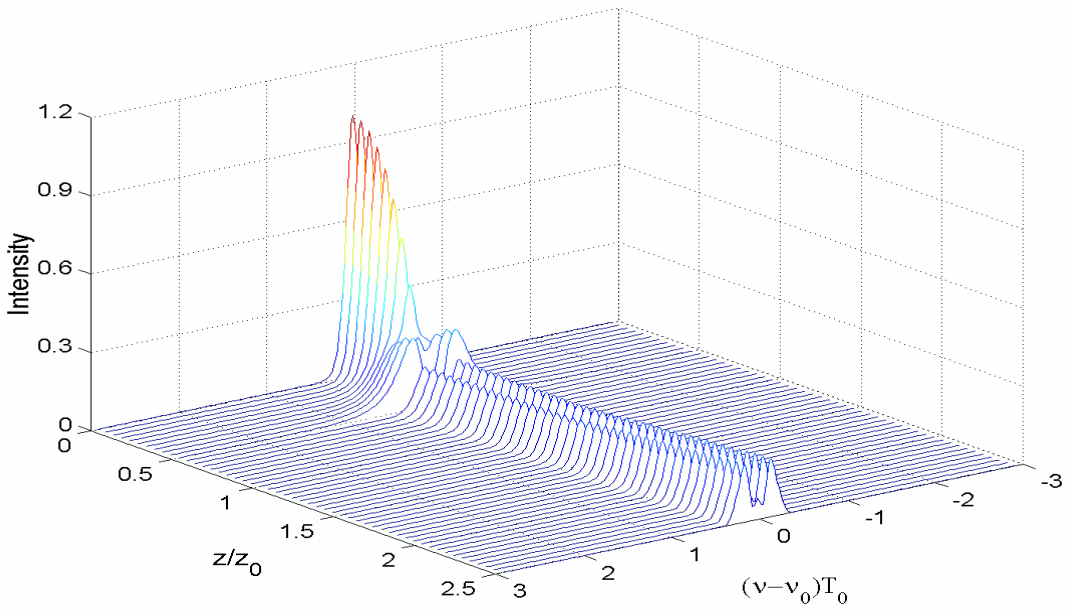

(b)

(b) Spectral evolution shows the formation of sub pulses at two wavelengths.

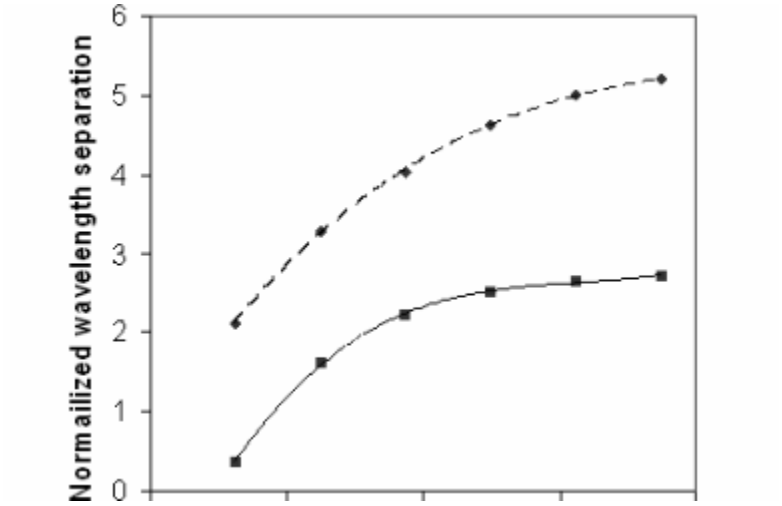
Normailized wavelength separation
0
1
2
3
4
5
6

(a)

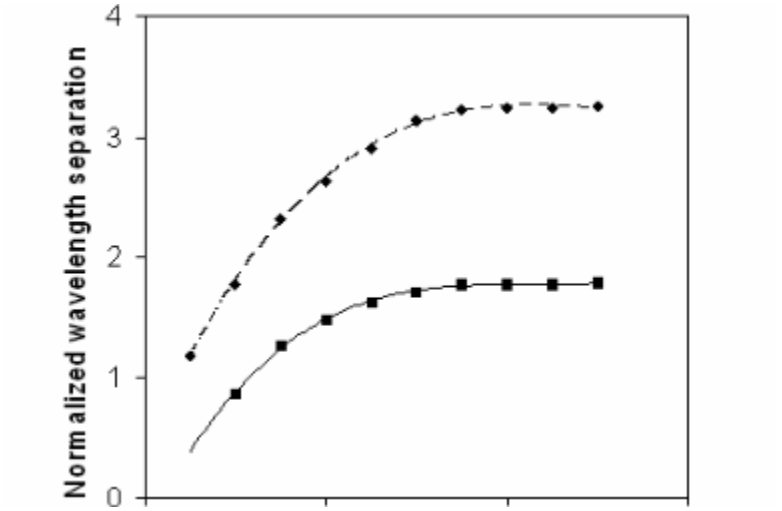
Normalized wavelength separation
0
1
2
3
4

(b)

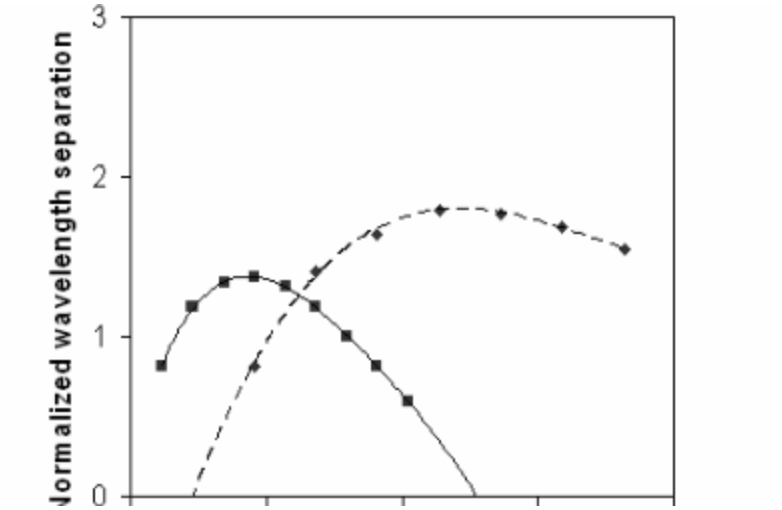
Normalized wavelength separation
0
1
2
3

(c)

FIGURE 3.9 Wavelength separations obtained as functions of dispersion difference (a), attenuation (b), and filter bandwidth (c) for N=2 solitons (solid curves) and N=3 solitons (dashed curves). Wavelength separation and filter bandwidth are normalized with respect to the input FWHM spectral width.

Higher-Order Effects

When pulse widths are reduced to values on the order of a few picoseconds or less, the higher order terms in Equation (2.2.6) involving δ, s, and τ R can become appreciable and may lead to degradation of the signal after the perturbation. These were studied for the N =2 soliton case. The most important of the three, appearing with input pulse widths of ΔTf =1 ps and shorter, is Raman scattering; this has the effect of shifting energy from the shorter wavelength into the longer wavelength pulse, leading to an amplitude imbalance between the two pulses, in a manner observed in non-perturbed N=2 solitons [11]. In addition, both pulses experience a self frequency shift to longer wavelengths. These effects, shown in Figure 3.7, become more pronounced as input pulse widths become shorter, and ultimately prevent sub-pulse evolution into fundamental solitons, as expected [10]. The cubic dispersion term was found to introduce a slight asymmetry in the overall signal envelope which tends to counter-act the imbalance arising from the Raman effect. This effect, observed previously in N=2 solitons [21], imparts a slight correction to the Raman imbalance, but again is negligible for pulse widths of 1 ps and longer. The self steepening term was found to have a negligible effect for pulse widths above ΔTf =0.1 ps. All three processes are thus avoided for N=2 solitons with input pulse widths of ΔTf >1 ps.

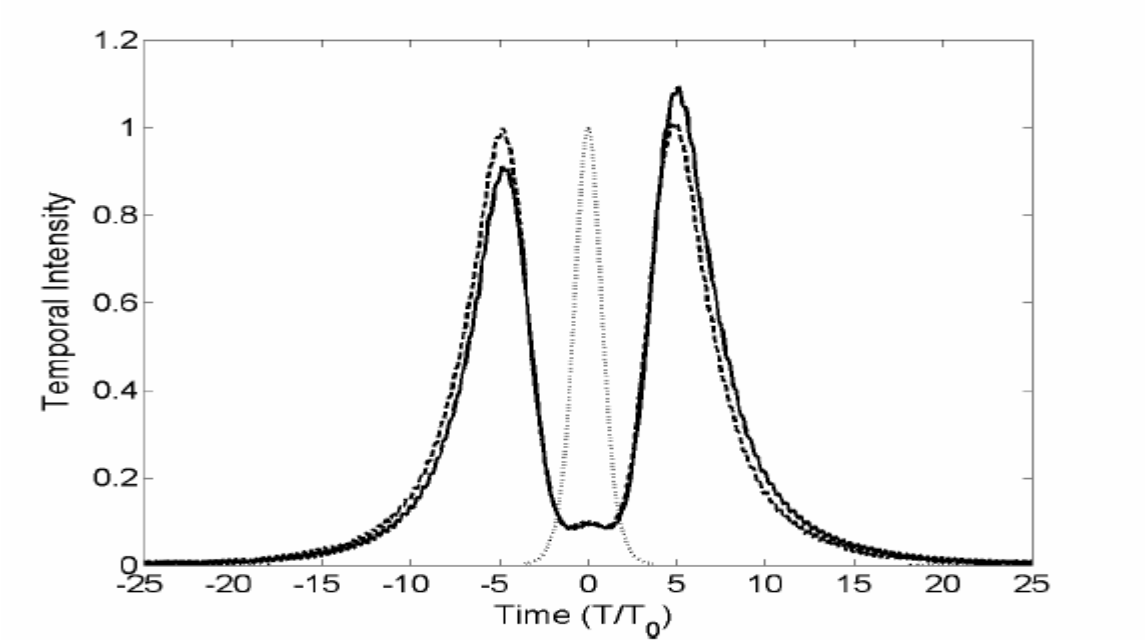

(a)

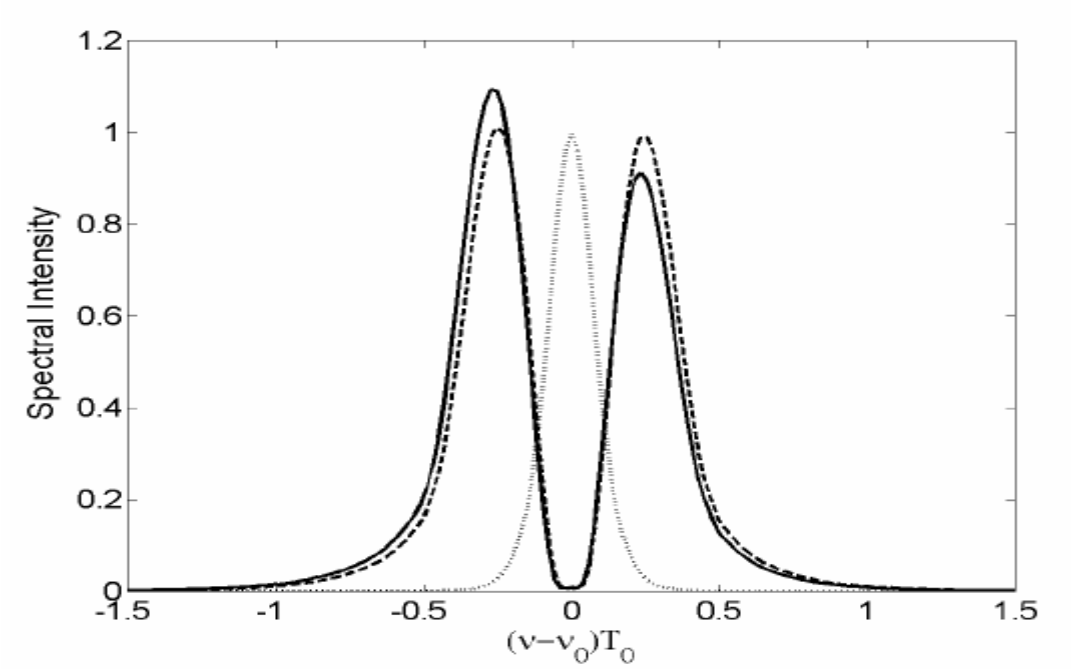

(b)

FIGURE 3.10a Normalized temporal plots showing the effects of cubic dispersion and Raman scattering on the separated pulses after stepping up the dispersion. The dotted traces are those of the input pulse. Solid traces correspond to a 10 ps input pulse width. Dashed traces correspond to a 1 ps input width.

CHAPTER 4

EXPERIMENTS ON WAVELENGTH CONVERSION USING *N*=2 SOLITON DECAY

4.1 Introduction

In the previous chapter, the decay of higher order solitons in optical fiber, initiated by a step change in dispersion or by a localized loss element or filter, is explored numerically as a means of generating pairs of pulses having wavelengths that are up and down-shifted from the input wavelength. The wavelengths are tunable by varying the magnitude of the perturbation. In this chapter, we propose a tunable wavelength conversion method using the controlled decay of N=2 solitons. Tunable wavelength conversion using N=2 soliton decay initiated by a step change in dispersion will be demonstrated experimentally. Obtainable wavelength separations as a function of the dispersion difference will be measured for a 1 ps soliton pulse. Stability of the wavelength conversion process will be investigated.

4.2 Experiments Using a Step Change in Dispersion

We have shown that the higher-order soliton decay initiated by localized channel perturbations could generate pairs of pulses having wavelengths that are up and downshifted from the input wavelength. Using the higher-order soliton decay, it is possible to generate two copies of an optical data stream, in which the copies are at wavelengths that differ from that of the original data. This proposed wavelength conversion method is very simple and in principle error-free. The process can in principle be repeated to produce multiple wavelength replicas of an input data stream, and may thus be of possible use in multi-casting applications in fiber communication systems. In this section, we experimentally demonstrate a tunable wavelength conversion using N=2 soliton decay initiated by a step change in dispersion.

Figure 4.1 shows the experimental setup for N=2 soliton decay. A figure-8 laser (F8L) is used to produce a soliton pulse. The 1-ps FWHM output from a figure-8 laser (F8L) was amplified by an erbium-doped fiber amplifier (EDFA) and then launched at location A such that its pulse width and intensity satisfied the N=2 soliton condition within the initial low-dispersion fiber (LDF) section. The center wavelength was 1550 nm and the peak power was 36 W. The amplifier introduced low-level spectral features on the pulse that are associated with amplified spontaneous emission (ASE). Simulations showed these features to have negligible effect on the pulse evolution. For a transition to higher dispersion fiber at one-half the soliton period for N=2, we use a half soliton period of a low dispersion fiber (LDF) and two soliton periods of a corning SMF-28 fiber. The dispersion parameter of the LDF at 1550 nm is 4.3 ps/km/nm, and its mode field diameter (MFD) is 8.4 μ m. For the SMF-28, the dispersion parameter at 1550 nm is 17 ps/km/nm, and its MFD is 10.4 μ m. Using a transition to a higher dispersion fiber effectively reduces the value of N while maintaining the pulse energy. The result is the formation of two fundamental solitons at the separate wavelengths.

Autocorrelation traces and spectral measurements at each stage (from locations A to C) are shown in Figure 4.2, along with results of the numerical simulations for a 1 ps (FWHM) N=2 soliton with ΔD = 75%. Measurements at position B confirmed the expected N=2 soliton temporal compression and spectral separation at the z0/2 location. The increase in dispersion to 17 ps/nm-km at B lowers the nonlinear response in the B-C segment, allowing the two sub-pulses to temporally separate and dispersively broaden, as confirmed by the autocorrelation measurement at position C. These results were found to be in excellent agreement with numerical simulations, shown as the dashed traces in Figure 4.2. The spectrum at point B (z=0.5z0) shows the maximum wavelength separation. Measured and simulated maximum wavelength separations are 6.2 nm and 6.9 nm respectively. About a 10 dB dip is observed between the two separated wavelength components. The measured autocorrelation trace at position C in Figure 4.2 shows 3 peaks, which confirms that two sub-pulses

are formed at this position. Measured and simulated wavelength separations between two subpulses at the end of the SMF-28 are 6.1 nm and 6.7 nm respectively.

Wavelength separations at position C as a function of the dispersion difference are measured at three data points. They are plotted in Figure 4.3 for the N=2 soliton case. The solid curve indicates a simulation result. The wavelength separation is normalized with respect to the input spectral width (in turn inversely proportional to the input pulse width). The experimental results are in a good agreement with the simulation results.

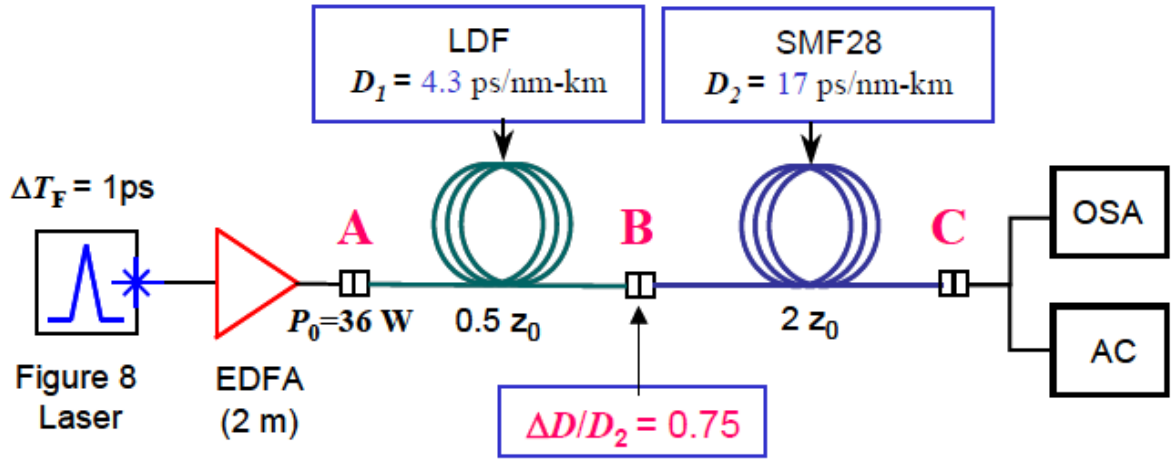

FIGURE 4.1 Experimental setup for N=2 soliton decay using a step increase in dispersion; OSA: Optical Spectrum Analyzer and AC: Auto-Correlator.

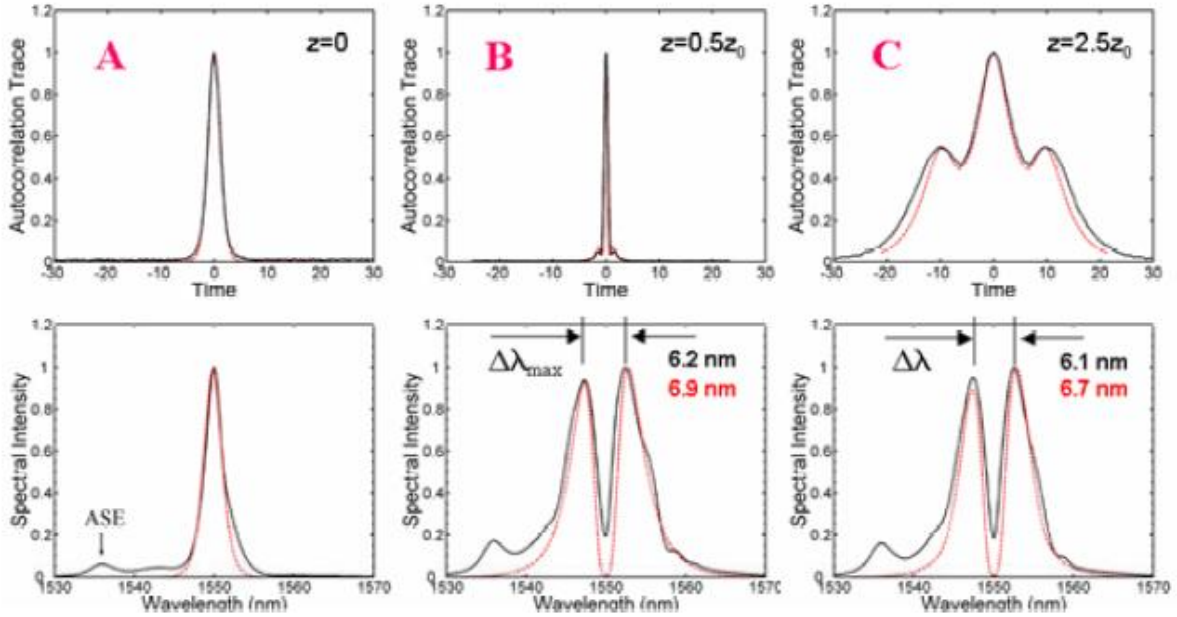

FIGURE 4.2 Measured (solid line) and simulated (dashed line) autocorrelation traces and spectra at the z/z0= 0, 0.5, and 2.5 for a 1 ps (FWHM) N=2 soliton with ΔD = 75%.

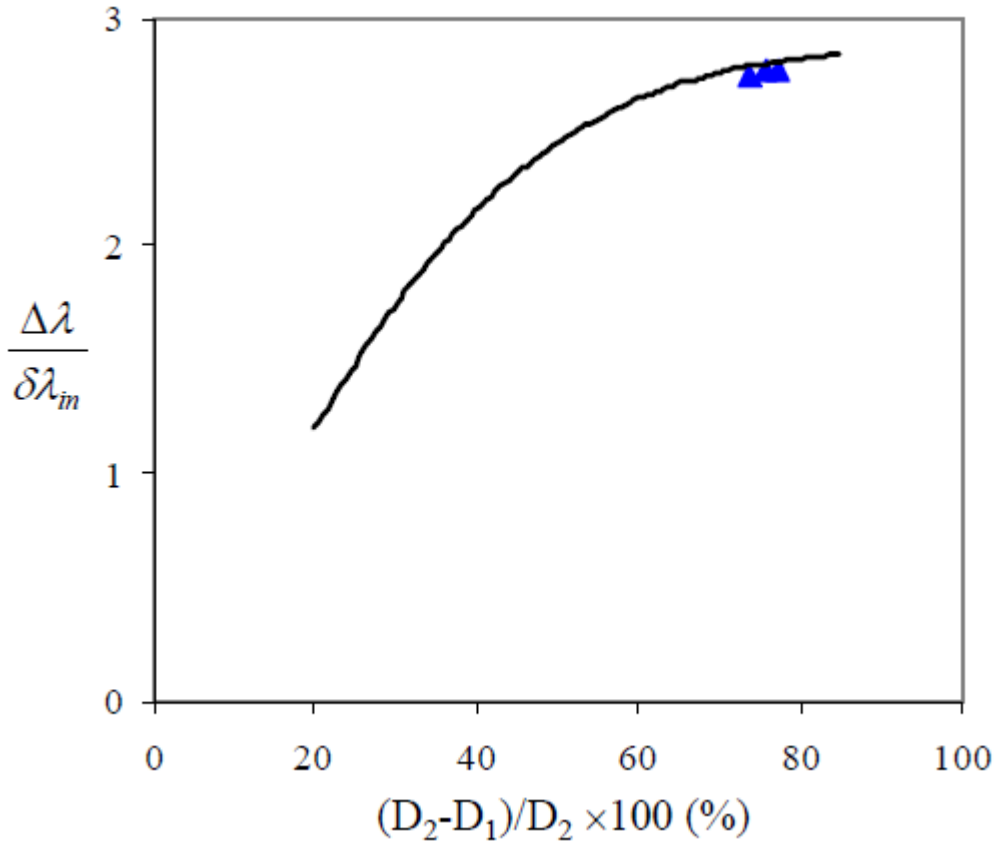

FIGURE 4.3 Measured wavelength separations as function of dispersion difference; solid line indicates a simulation result. The wavelength separation is normalized with respect to the input spectral width

4.3 Stability of Wavelength Conversion

In this section, stability or robustness of the wavelength conversion process will be investigated. The main emphasis is on the sensitivity of wavelength separation to fluctuations in power and/or variations in the perturbation locations in the fiber channel. For practical applications of the proposed wavelength conversion method, stability or robustness of the system is an important factor. Figure 4.4 shows the simulation and experimental studies on the sensitivity of wavelength separation to power fluctuations in the fiber channel. An input power decrease by a given percentage results in approximately twice that percentage decrease in spectral separation. Increasing the input power beyond the *N*=2 condition slightly increases the

spectral separation, which eventually saturates to a maximum. Therefore, the sensitivity of the system to power fluctuations in the fiber channel can be decreased significantly by operating the wavelength conversion in the saturation region. Discrepancy between measured and simulated wavelength separation increases as the input power increases. This may result from using larger Raman response parameters in the simulation because the effect of stimulated Raman scattering on wavelength separation tends to increase wavelength separation when the input power is high.

The perturbation location in practical implementation may differ from the theoretical location, where the maximum wavelength separation occurs (seen in Figure 4.1). The simulation studies on the sensitivity of wavelength separation to variations in the perturbation locations in the fiber channel have been performed.

The resulting wavelength separations are seen to change slightly (within ± 10 percent). This result shows that the system is robust to variations in perturbation location in the fiber channel. The effect of using non-soliton pulses, whose pulse shapes and spectra may differ from those of the exact soliton, on wavelength separation has also been determined.

4.4 Fundamental and higher order solitons

This demonstrates that the exact balance between the effects of SPM and GVD leads to the formation of a fundamental soliton - a light pulse that propagates without changing its shape and spectrum, and shows some basic features of the higher-order solitons.

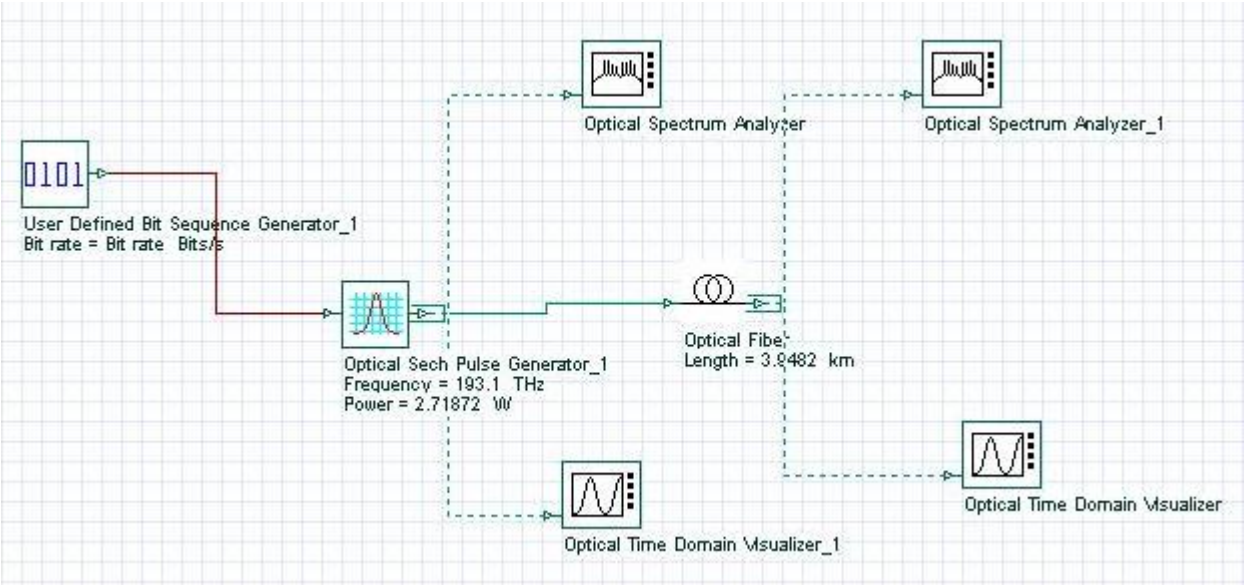

Figure 4.5: System Layout

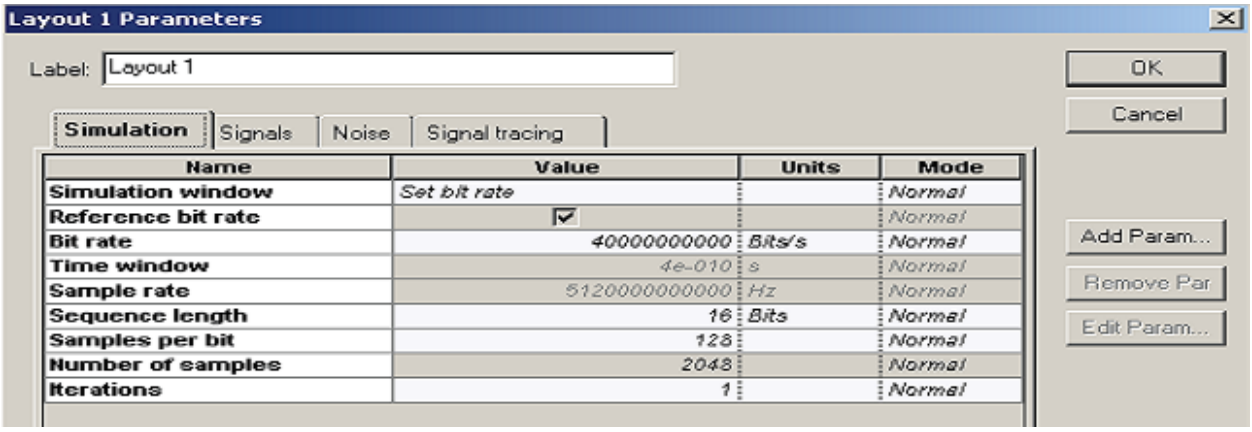

Figure 4.6: System Parameters

The compensation between the effects of SPM and GVD is not complete for Gaussian pulses since the SPM induced chirp is different from that induced by the GVD. The exact compensation occurs when the pulse shape is that of a fundamental soliton.

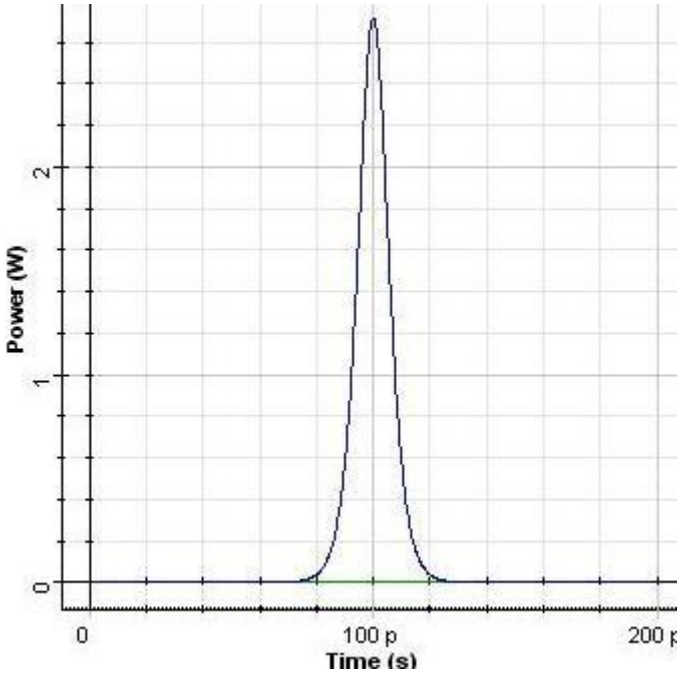

Figure 4.7: optical time domain visualize

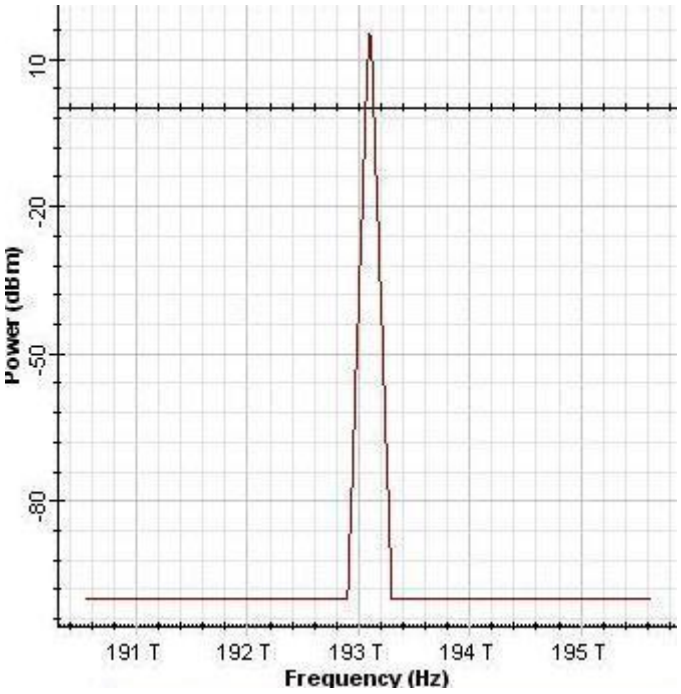

Figure 4.8: optical spectrum analyzer

Output Pulse Shapes corresponding to the fundamental (N=1) soliton over one soliton period.

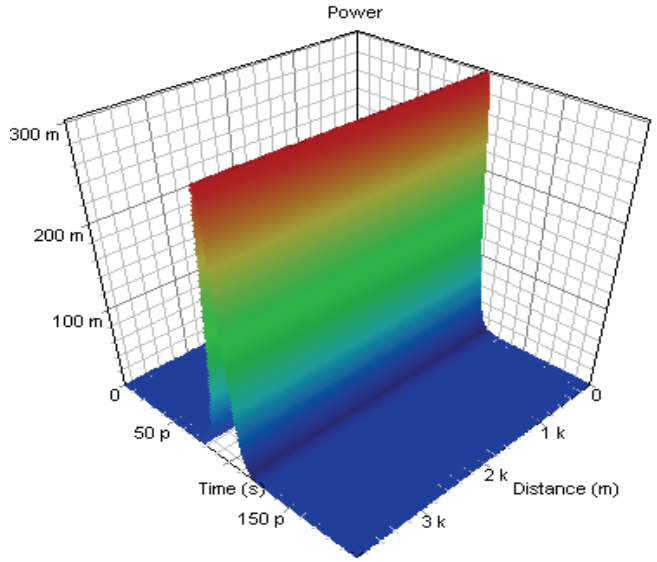

Figure 4.9: Optical time domain visualize

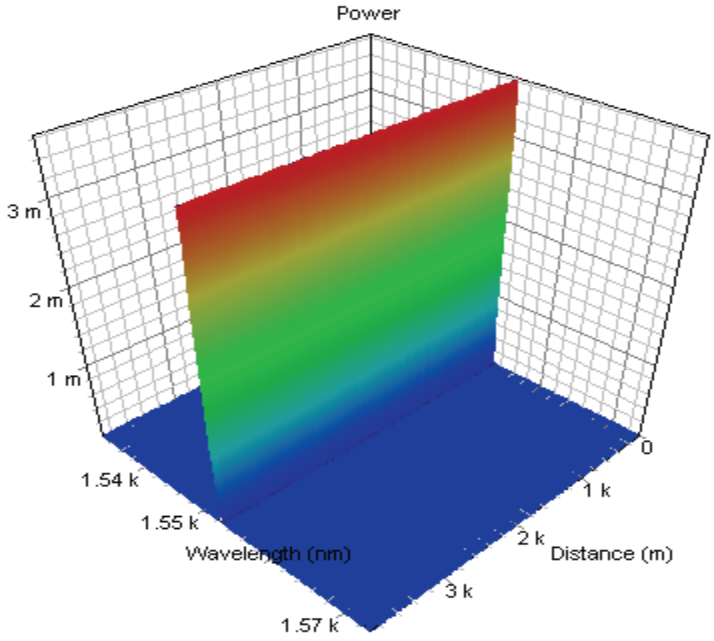

Figure 4.10: Optical spectrum analyzer

Output Pulse Shapes corresponding to the fundamental (N=2) soliton over one soliton period.

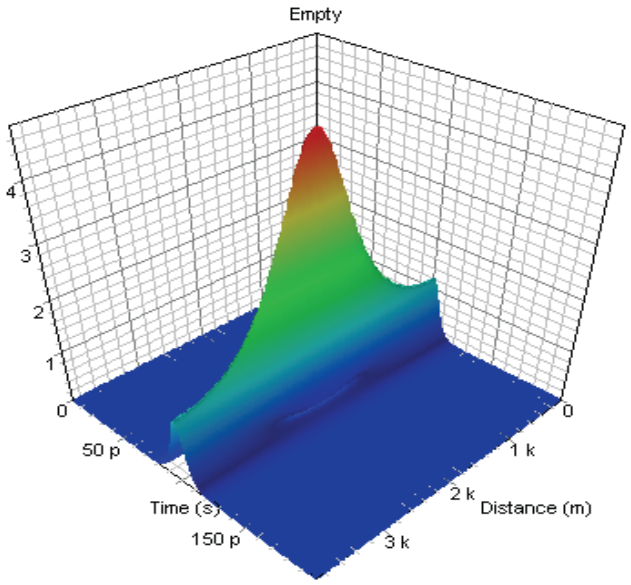

Figure 4.11: Optical time domain visualize

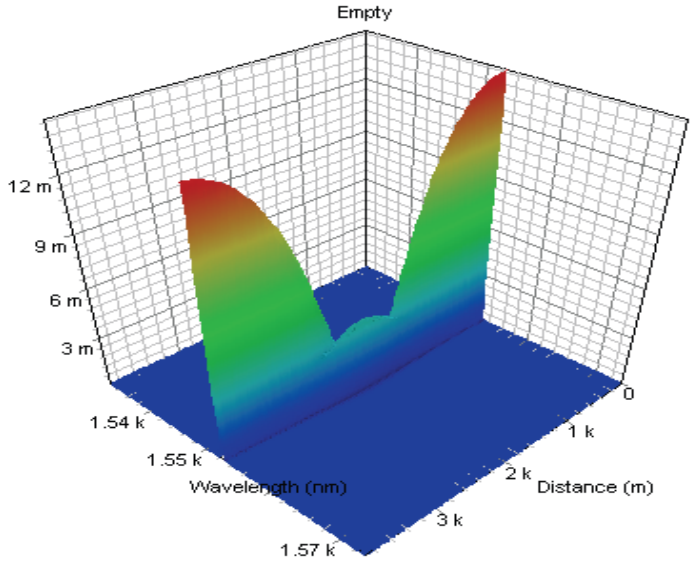

Figure 4.12: Optical spectrum analyzer

4.5 Solitons Self-steepening Decay of N=2 Soliton

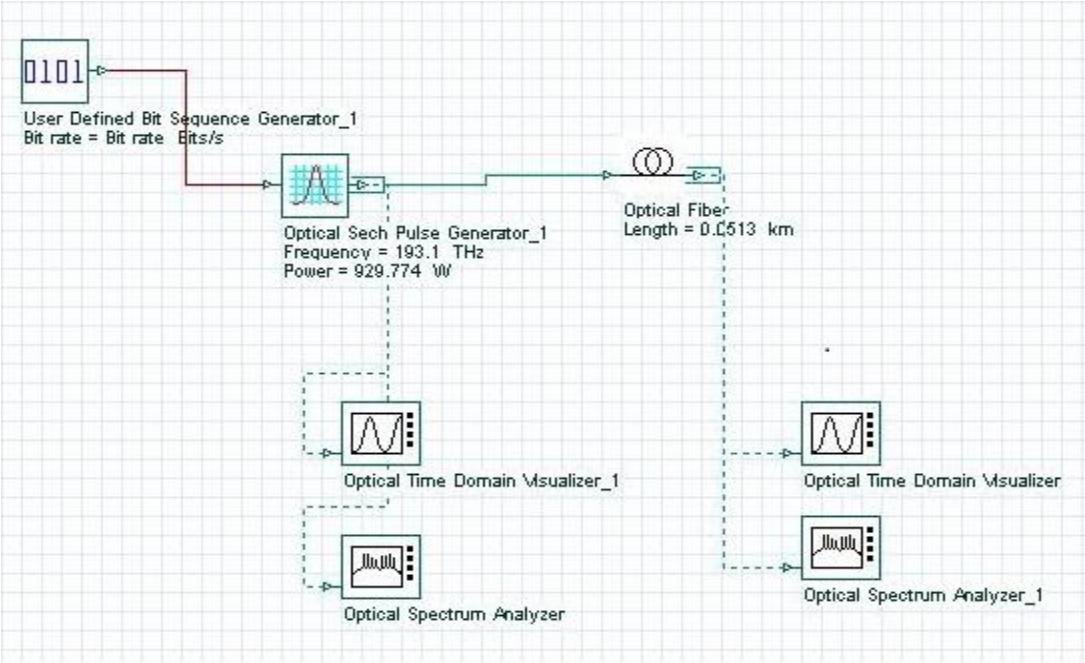

Figure 4.13: System Layout

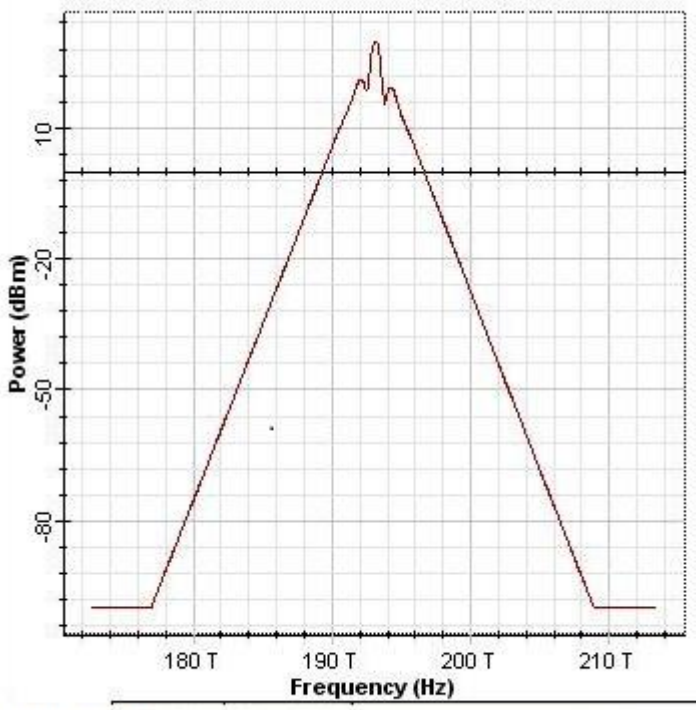

Fig. 4.14: Optical Spectrum Analyzer_1

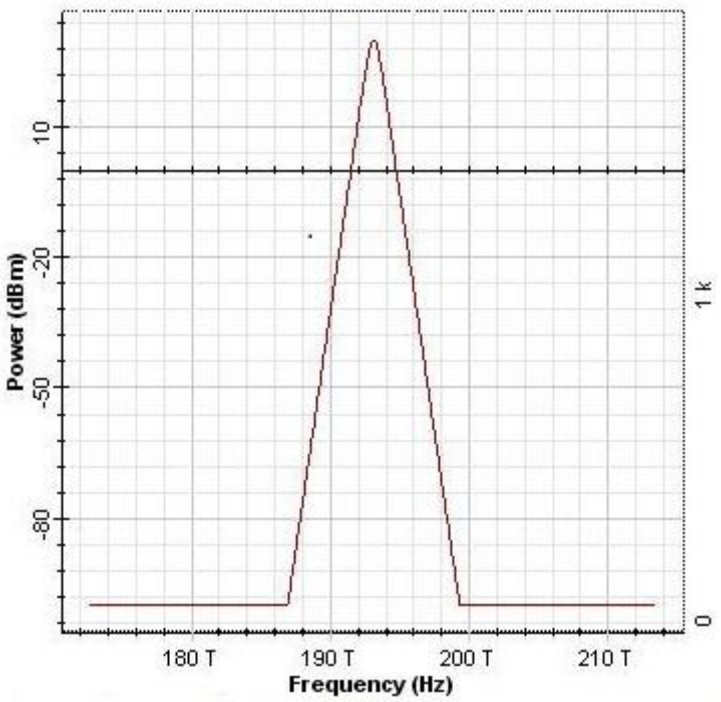

Fig. 4.15: Optical Spectrum Analyzer

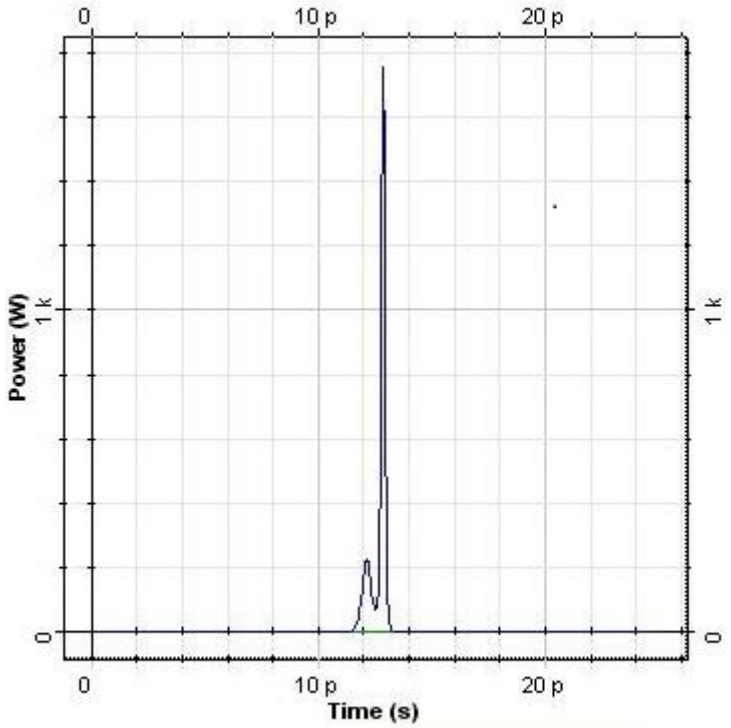

Fig. 4.16: Optical Time Domain Visualizer

4.6 Solitons Decay of N=2 soliton caused by Raman Scattering

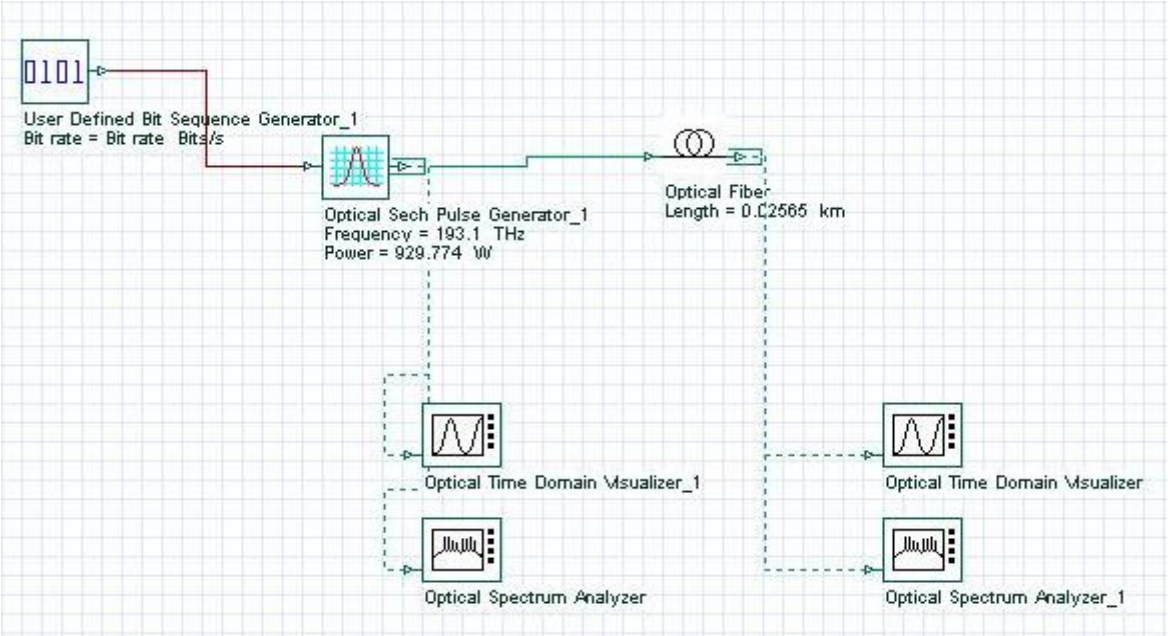

Figure 4.17: System Layout

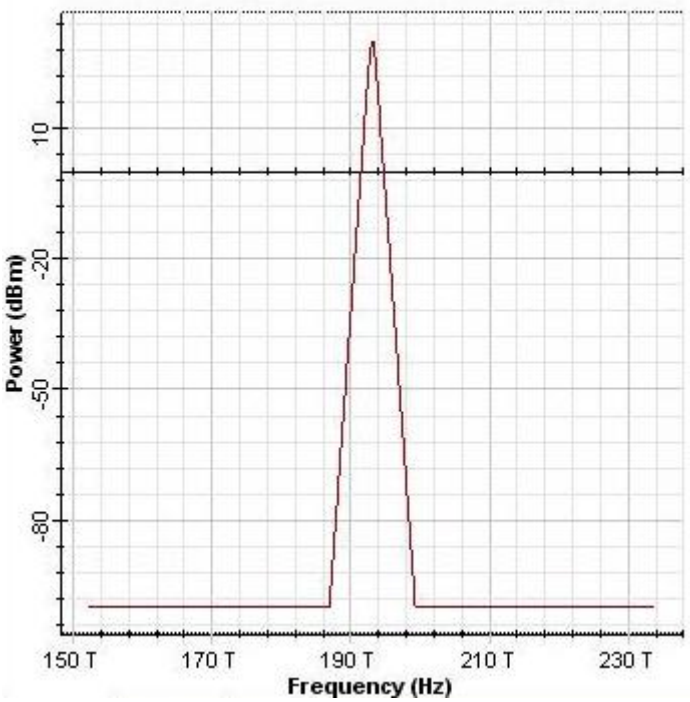

Figure 4.18: Optical Spectrum Analyzer

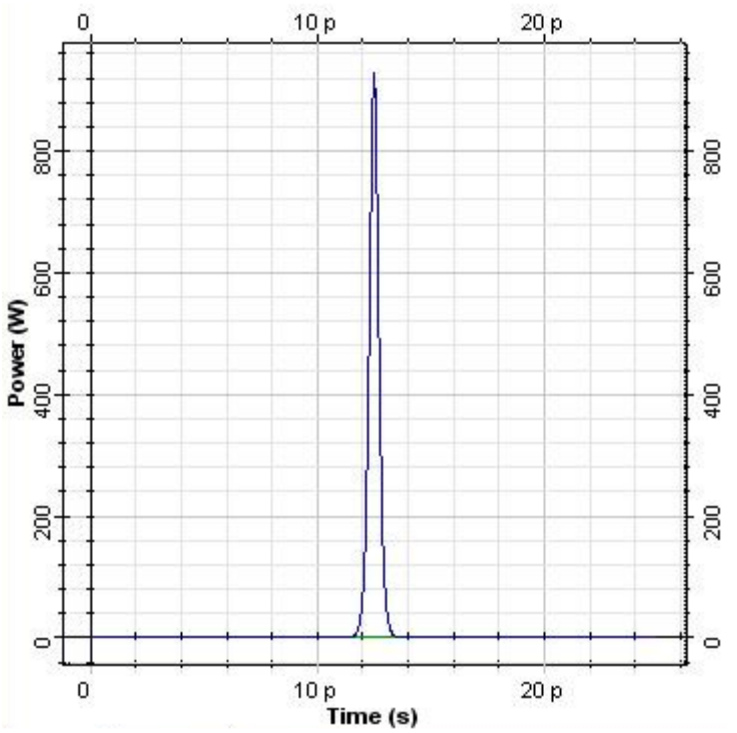

Figure 4.19: Optical Time Domain Visualize

CHAPTER 5

CONCLUSION

The object of this research was to investigate the decay and recovery of higher-order solitons initiated by localized channel perturbation. A detailed modeling effort for soliton propagation in optical fibers was performed to accomplish this task. A simulation tool was developed using split step Fourier method (SSFM). The higher-order soliton decay initiated by a localized channel perturbation in the fiber channel has been demonstrated theoretically and experimentally as a means of generating pairs of pulses having wavelengths that are up and down-shifted from the input wavelength. Other effects such as Raman scattering and cubic dispersion were shown to de-stabilize the process, but can be minimized by operating with pulse widths of the order of 1 ps or longer. Recovery of the original pulse by applying a reverse perturbation down-channel was also found to be feasible, provided dispersion in the channel between perturbations is compensated, and that higher order dispersion and nonlinearities are low. The separated pulses at two wavelengths can in principle be amplified to form separate higher order solitons. The process is repeated to produce multiple wavelength replicas of an input data stream, and may thus be of possible use in multi-casting applications in fiber communication systems.

We have shown that the spectral separation effect in N=2 solitons can be used as a method of converting a single pulse into two sub-pulses at displaced wavelengths by incorporating a dispersion step at the half soliton period location. Wavelength shifts are tunable by varying the magnitude of the dispersion step, or by varying the input pulse power above or below that required for the N=2 soliton condition. The method may find applications in WDM data transmission, in those two wavelength-converted

replicas of a single data stream can be generated. Proposed applications have been presented for the wavelength separation and recovery processes.

REFERENCES

[1] J. Hecht, *City of Light* (Oxford University Press, New York, 1999).

[2] J. L. Baird, British Patent 285,738 (1928).

[3] C. W. Hansell, U. S. Patent 1,751,584 (1930).

[4] H. Lamm, *Z. Instrumenten.* **50**, 579 (1930).

[5] A. C. S. van Heel, *Nature* **173**, 39 (1954).

[6] H. H. Hopkins and N. S. Kapany, *Nature* **173**, 39 (1954); *Opt. Acta* **1**, 164 (1955).

[7] B. O'Brian, U. S. Patent 2,825,260 (1958).

[8] B. I. Hirschowitz, U. S. Patent 3,010,357 (1961).

[9] N. S. Kapany, *Fiber Optics: Principles and Applications* (Academic, New York, 1967).

[10] K. C. Kao and G. A. Hockham, *IEE Proc.* **113**, 1151 (1966).

[11] F. P. Kapron, D. B. Keck, and R. D. Maurer, *Appl. Phys. Lett.* **17**, 423 (1970).

[12] W. G. French, J. B. MacChesney, P. B. O'Connor, and G. W. Tasker, *Bell Syst. Tech. J.* **53**, 951 (1974).

[13] T. Miya, Y. Terunuma, T. Hosaka, and T. Miyashita, *Electron. Lett.* **15**, 106 (1979).

[14] I. P. Kaminow and T. L. Koch (eds.), *Optical Fiber Telecommunications III* (Academic Press, San Diego, CA, 1997).

[15] G. P. Agrawal, *Fiber-Optic Communication Systems*, 2nd ed. (Wiley, New York, 1997).

[16] R. Ramaswami and K. Sivarajan, *Optical Networks* (Morgan Kaufmann, Burlington, MA, 1998).

[17] G. Keiser, *Optical Fiber Communications*, 3rd ed. (McGraw-Hill, New York, 2000).

[18] R. H. Stolen, E. P. Ippen, and A. R. Tynes, *Appl. Phys. Lett.* **20**, 62 (1972).

[19] E. P. Ippen and R. H. Stolen, *Appl. Phys. Lett.* **21**, 539 (1972).

[20] R. G. Smith, *Appl. Opt.* **11**, 2489 (1972).

[21] R. H. Stolen and A. Ashkin, *Appl. Phys. Lett.* **22**, 294 (1973).

[22] R. H. Stolen, J. E. Bjorkholm, and A. Ashkin, *Appl. Phys. Lett.* **24**, 308 (1974).

[23] K. O. Hill, D. C. Johnson, B. S. Kawaski, and R. I. MacDonald, *J. Appl. Phys.* **49**, 5098 (1974).

[24] R. H. Stolen, *IEEE J. Quantum Electron.* **QE-11**, 100 (1975).

[25] R. H. Stolen and C. Lin, *Phys. Rev. A* **17**, 1448 (1978).

[26] A. Hasegawa and F. Tappert, *Appl. Phys. Lett.* **23**, 142 (1973).

[27] L. F. Mollenauer, R. H. Stolen, and J. P. Gordon, *Phys. Rev. Lett.* **45**, 1095 (1980).

[28] L. F. Mollenauer and R. H. Stolen, *Opt. Lett.* **9**, 13 (1984).

[29] L. F. Mollenauer, J. P. Gordon, and M. N. Islam, *IEEE J. Quantum Electron.* **QE-22**, 157 (1986).

[30] J. D. Kafka and T. Baer, *Opt. Lett.* **12**, 181 (1987).

[31] E. A. Golovchenko, E. M. Dianov, A. M. Prokhorov, and V. N. Serkin, "Decay of optical solitons," JETP Lett. 42, 87-91, 1985. Referrence

[32] K.Ohkuma, Y.H. Ichikawa, and Y.Abe, "Soliton propagation along optical fibers", Opt. Lett., 12, 516-518, 1987.

[33] Kuochou Tai and Akira Hasegawa, "Fission of optical solitons induced by stimulated Raman effect", Opt. Lett. 13, 392-394, 1988.

[34] P. K. Wai, C. R. Menyuk, Y. C. Lee, and H. H. Chen, "Nonlinear pulse propagation in the neighborhood of the zero-dispersion wavelength of monomode optical fibers", Opt. Lett. 11, 464-466, 1986.

[35] S.R. Clarke, R.H.J. Grimshaw, and B.A. Malomed, "Soliton formation from a pulse passing the zero dispersion point in a nonlinear Schödinger equation", Phys. Rev. E 61, 5794-5801, 2000.

[36] K.-S. Lee, M.C. Gross, S.E. Ralph, and J.A. Buck, "Wavelength conversion using N=2 soliton decay and recovery in fiber, initiated by dispersion steps", IEEE Photonics Technol. Lett., vol. 16, no. 2, 2004.

[37] K.-S. Lee and J. A. Buck, "Wavelength conversion through higher-order soliton splitting initiated by localized channel perturbations", J. Opt. Soc. Am. B, vol. 20, no. 3, 2003.

[38] V. E. Zakharov and A. B. Shabat, "Exact theory of two-dimensional self-focusing and one-dimensional self-modulation of waves in nonlinear media," Sov. Phys. JETP 34, pp 62-70, 1972.

[39] J. Satsuma and N. Yajima, "Initial value problem of one-dimensional self-modulation of nonlinear waves in dispersive media," Prog. Phys. Suppl. 55, pp. 284-300, 1974.

[40] C.R. Menyuk, "Soliton robustness in optical fibers", J. Opt. Soc. Am. B 10, 1585-1591, 1993.

[41] W. Hodel, and H.P. Weber, "Decay of femtosecond higher-order solitons in an optical fiber induced by Raman self-pumping", Optics Lett., 12 924-926, 1987.

[42] John A. Buck, Fundamentals of Optical Fibers, Wiley Interscience, New York, 1995.

[43] E. Bourkoff, W. Zhao, R. I. Joseph, and D. N. Christodoulides, Opt. Lett. 12, 272, 1988.

[44] E. A. Golovchenko, E. M. Dianov, A. N. Pilipetskii, A. M. Prokhorov, and V. N. Serkin, JETP Lett. 45, 91, 1987.

[45] F. DeMartini, C. H. Townes, T. K. Gustafson, and P. L. Kelley, Phys. Rev. 164, 312, 1967.

[46] J. T. Manassah, M. A. Mustafa, R. A. Alfano, and P. P. Ho, IEEE J. Quantum Electron. QE-22, 197, 1986.

[47] P. Beaud, W. Hodel, B. Zysset, and H. P. Weber, IEEE J. Quantum Electron. QE-23, 1938, 1987.

[48] A.K. Atieh, P. Myslinski, J. Chrostowski, and P. Galko, "Measuring the Raman time constant for soliton pulses in standard single-mode fiber", J. Lightwave Tech., 17, 216-221, 1999.

[49] G.P. Agrawal, *Nonlinear Fiber Optics, 3rd ed*, Academic Press, San Diego, 2001.

[50] M. Nakazawa, H. Kubota, and K. Tamura, “Random evolution and coherence degradation of a high-order optical soliton train in the presence of noise”, Opt. Lett. 24, 318-320, 1999.

[51] P.L. François, “Nonlinear propagation of ultrashort pulses in optical fibers: total field formulation in the frequency domain”, J. Opt. Soc. Am. B, 8, 276-293, 1991.